Joint energy-efficiency communication optimization and perimeter traffic flow control for multi-region LTE-V2V networks

Jianshan Zhou, Guixia Qiu, Daxin Tian, Zhengguo Sheng, Xuting Duan, Yong Liang Guan, Victor CM Leung

Publication date

01-08-2023

Licence

Document Version

Accepted version

Published in

IEEE Transactions on Mobile Computing

Link to external publisher version

https://doi.org/10.1109/TMC.2023.3300311

Joint Energy-Efficiency Communication Optimization and Perimeter Traffic Flow Control for Multi-Region LTE-V2V Networks

Jianshan Zhou, Guixian Qu, Daxin Tian, *Senior Member, IEEE,* Zhengguo Sheng, *Senior Member, IEEE,* Xuting Duan, Yong Liang Guan, *Senior Member, IEEE,* and Victor C. M. Leung, *Life Fellow, IEEE*

Abstract—Energy-efficiency (EE) optimization of long-term evolution (LTE) networks dedicated to vehicle-to-vehicle communications (LTE-V2V) is critical for connected vehicles. In this paper, we integrate perimeter control methodologies from transportation science into EE optimization to make vehicular communications adaptive to temporal-spatial dynamics of macroscopic traffic flows in multiple urban regions. Specifically, we develop a hierarchical framework of joint LTE-V2V EE optimization and perimeter traffic flow control. Its goal is to minimize the total traffic network delay, defined as the integral of the vehicle accumulations in the urban regions over a prediction horizon time, meanwhile maximizing the energy efficiency of the LTE-V2V communications in the same regions. We propose a model predictive perimeter controller at a low level, using a macroscopic fundamental diagram (MFD) to capture the relationship between the traffic density and the outflow of each urban region. We also propose a high-level EE optimization model and an iterative algorithm, considering the multi-region coordinated traffic dynamics, to jointly optimize vehicular transmission power and beacon frequency. Simulation results validate our proposed models and show that our method outperforms the latest solutions by improving at least 9.57% EE of the multiple regions. Our method can also provide 27.69% improvement in resource utilization fairness, indicating a fairer EE performance distribution among these regions.

Index Terms—Long-term evolution network (LTE), energy efficiency (EE), perimeter control, vehicle-to-vehicle (V2V) communications.

1 INTRODUCTION

R ESOURCE management plays a critical role in the design and deployment of various wireless communications and networks, such as long-term evolution (LTE) networks that exploit device-to-device (D2D) features to realize vehicle-to-vehicle communications (LTE-V2V). Its fundamental goal is to optimize the achievable capacity and transmission performance of a communication system consuming a unit of energy resource, i.e., energy-efficiency (EE) optimization. LTE-V2V networks are considered a critical enabling component of intelligent transportation systems (ITS) in the future, promising a wide variety of vehicular safety applications, such as real-time beaconing in vehicular cooperative awareness [1]–[3]. However, the system-level performance of large-scale LTE-V2V communications

- *Jianshan Zhou, Daxin Tian, and Xuting Duan are with State Key Lab of Intelligent Transportation System, Beijing Key Laboratory for Cooperative Vehicle Infrastructure Systems & Safety Control, the School of Transportation Science and Engineering, Beihang University, Beijing 100191, China (e-mail: jianshanzhou@foxmail.com, dtian@buaa.edu.cn, duanxuting@buaa.edu.cn).*
- *Guixian Qu is with the Aero-engine System Collaborative Design Center, Research Institute of Aero-Engine, Beihang University, Beijing 100191, China (e-mail: guixianqu@foxmail.com).*
- *Zhengguo Sheng is with the Department of Engineering and Design, University of Sussex, Richmond 3A09, UK (e-mail: z.sheng@sussex.ac.uk).*
- *Yong Liang Guan is with the School of Electrical and Electronic Engineering, Nanyang Technological University, Block S1-B1c-106, Nanyang Avenue, 639798, Singapore. (Email: eylguan@ntu.edu.sg).*
- *Victor C. M. Leung is with Department of Electrical and Computer Engineering, the University of British Columbia, Vancouver, B.C., V6T 1Z4 Canada (e-mail: vleung@ieee.org).*

(Corresponding author: Guixian Qu)

is usually limited due to constrained LTE resource blocks (RBs) [4]. Recent studies [5]–[7] have demonstrated that physical-layer communication interferences and collisions may become more severe in road traffic scenarios with higher vehicle density. Generally, when the total traffic accumulation in an urban region increases, the average number of LTE-V2V communication vehicles in the same region rises, leading to the fact that the LTE RBs are insufficient to support the connected vehicles in the reuse range [8], [9]. The dynamical allocation of limited RBs among vehicles located within the same resource reuse range of an LTE-V2V communication network in an urban region, determining the LTE-V2V communication performance, directly depends on the vehicle density distribution and macroscopic traffic flow dynamics in this region. At this point, the evolution of the region-level traffic flow can significantly influence the system-level performance of the LTE-V2V network.

Additionally, an urban road area can be partitioned into several adjacent regions to facilitate real-time road traffic management and control of the large-scale urban road traffic network. It is recognized from considerable studies (such as [10]–[14]) in transportation science that the temporal-spatial dynamics of macro-level traffic flows in the adjacent regions is highly coupled. Thus, the performance of the LTE-V2V network in each region is inherently coupled with that in other neighboring regions since each region's vehicle density relies on the internal traffic generation and the flow transferring between the neighboring regions. From the system-level perspective, optimizing multi-region LTE-V2V networks requires understanding the relationship of multi-region macroscopic traffic dynamics and how to adapt the

resource allocation of the communication networks to the macroscopic traffic dynamics.

Nevertheless, few current efforts (to the best of our knowledge) have been made to incorporate multi-region macroscopic traffic dynamics into an LTE-V2V network optimization framework. While many resource allocation methods and application frameworks of cellular vehicular networks, such as [15]–[18], can provide high energy efficiency in a low-density traffic region, their global optimization performance regarding multiple neighboring regions may be limited because their lack of coordinating inter-region transfer flow dynamics produces an imbalanced temporal-spatial distribution of multi-region vehicle densities. Most state-of-the-art resource optimization methods in wireless communication and networks focus on communication systems but have not incorporated the impact of road traffic systems on their communication systems and cannot provide multi-disciplinary insight and design. The absence of integrating road traffic control tools into communication optimization and resource management for connected vehicles, yielding poor communication performance in some congested urban regions, limits the overall performance of communication networks deployed in multiple regions.

Meanwhile, in the transportation community, advanced perimeter control approaches like [19]–[21] have been proposed to regulate the traffic flows (i.e., vehicle flows) transferring between neighboring urban regions. Recent perimeter control frameworks generally build on the principle of macroscopic fundamental diagram (MFD) that is used to describe the aggregated road traffic dynamics and provides the relationship between vehicle density and space-mean traffic flow or output flow of an urban region at an aggregated scale [22]–[25]. These studies show that the MFD provides a powerful modeling tool to develop tractable dynamical system models for multi-region road traffic dynamics and to design region-level flow control schemes for coordinating the traffic dynamics of these regions. Such traffic control schemes with MFD motivate a potential progress towards a new generation of joint management and optimization of vehicular networks and urban road traffic flows. Nevertheless, it remains unexplored how to integrate multi-region traffic dynamics under MFD-based perimeter control into the EE optimization of multi-region vehicular networks.

In this paper, we propose a hierarchical joint optimization framework for coordinating traffic flow dynamics of multiple adjacent regions to alleviate traffic congestion or unbalanced traffic distribution over the regions and for improving the EE performance of the LTE-V2V networks in the corresponding regions simultaneously. This framework leads to a joint vehicular communication optimization and macroscopic traffic control (VCOMTC) methodology. The lower level of the framework proposes a nonlinear model predictive controller (MPC) based on the multi-region MFDs to realize optimal perimeter control, i.e., manipulating traffic flows transferring between neighboring regions. We further develop a vehicular EE communication optimization model and an effective solving algorithm that incorporates the multi-region traffic dynamics coordinated by the lower-level MFD-based MPC model, thus enabling the adaptive response of the multi-region LTE-V2V networks to the temporal-spatial evolution of traffic flows in the regions.

With the above hierarchical framework, we provide a critical insight into how multi-region LTE-V2V networks can benefit from integrating traffic dynamics control and EE communication optimization, facilitating interdisciplinary research from transportation and communication domains.

1.1 Literature Review

Recently, integrating advanced information communication technologies, such as network function virtualization (NFV), central and edge clouds, mobile edge computing (MEC), and 5G network architecture, with vehicular communications has spawned new implementation architectures for vehicular networks like 5G vehicular networks [15]. This advancement is believed to provide opportunities to transform traditional vehicles and cities into smart ones. To practically enable vehicle-to-everything (V2X) communications based on current radio access technologies, many research efforts develop different mobility management models and protocols to improve seamlessness, reliability, and throughput of the network systems such as Dedicated Short Range Communications (DSRC), LTE, and 5G networks [16]. Representative state-of-the-art mobility management schemes include software-defined networks (SDN)-based, fog-based, and heterogeneous networks-based methods [16]. However, due to the limitation of radio resources, large-scale deployment of vehicular networks will meet some significant challenges, among which increasing wireless interference and transmission collisions is an essential issue. Traditional solutions to this issue are modifying existing medium access control (MAC) protocols like carrier sense multiple access with collision avoidance (CSMA/CA) protocols or designing novel physical-layer congestion control schemes. For example, many researchers from the communication community have developed different congestion control schemes, such as rate adaption- or power adaption-based control approaches, joint power and rate optimization approaches, and non-orthogonal multiple access (NOMA)-based methods [17]. As LTE-based and 5G New Radio (NR)-based access technologies are two main streams of cellular V2X (C-V2X) networks, many recent sidelink resource allocation frameworks aim to improve the performance of dynamic scheduling and sensing-based semi-persistent scheduling (SB-SPS) algorithms operated in LTE-V2X Mode 3 and Mode 4 and extend these scheduling algorithms to the counterparts (i.e., Mode 1 and Mode 2) in 5G-V2X networks [18]. These frameworks modify the legacy SB-SPS procedure by combining other enhancement mechanisms, such as variable-size packet design, reservation splitting, long blind spot avoidance, and position- and mobility-aware optimization, with the resource scheduling algorithms in LTE-V2X or 5G-V2X networks [18].

The existing surveys [15]–[18] show that many resource allocation schemes can provide better connectivity and resource utilization, while they also suggest that much space remains to improve C-V2X networks. The underlying idea is to enable resource allocation procedures to adapt to time-varying environmental conditions (e.g., road traffic flows and vehicle density). However, while region-level road traffic dynamics characterizes varying vehicle density that affects the resource utilization of either LTE-V2X or 5G-V2X

networks, few existing resource scheduling schemes have integrated macroscopic road traffic management and control into their radio resource allocation. It is left to establish the connection between the EE optimization of multi-region vehicular networks and traffic dynamics.

Approaches based on convex approximation, mixed integer programming, and learning-based optimization techniques have been developed for maximizing network-wide EE performance of vehicular networks [26]–[30]. Other approaches to optimize the EE performance of vehicular networks follow a joint control framework of power and beacon rate [31]–[40]. These approaches can be divided into three main categories, including i) mathematical optimization-based approaches that formulate the joint resource allocation problem as multi-stage optimization problems [31], [36], mixed boolean linear programming problems [33] or mixed integer nonlinear programming problems [40], ii) learning-based approaches such as Q-learning [32], federated learning [34], and Deep Deterministic Policy Gradient (DDPG) schemes [37], and iii) game-theoretical approaches such as [38], [41], [42]. In [35], the researchers analytically derive packet reception probability (PRP) of resource allocation algorithms for LTE-V2V networks, providing an insight into the effect of application-layer and physical-layer parameters on the network performance. As fairness is another significant optimization objective in resource allocation, [43] provides a general model describing the tradeoff between the optimal performance of a multi-user wireless communication system and its achievable fairness in resource allocation. This theoretical model can pave the way for designing optimal EE-fairness tradeoff schemes. In [44], the researchers propose a power control approach based on Channel Busy Ratio (CBR) measurement to enhance the fairness of radio resource allocation among vehicles broadcasting messages via the DSRC network. Additionally, other researchers move towards improving fairness among vehicles while optimizing radio resource usage via adaptive clustering and cluster head selection [39].

The above literature shows that various optimization schemes succeed in power control, rate adaptation, and joint resource allocation of vehicular networks. However, these existing studies mainly focus on communication modeling and optimization of single-region vehicular networks, neglecting the impact of multi-region road traffic flow dynamics on the communication system. Even though they recognize that spatial vehicle density distribution significantly influences the usage of radio resources in vehicular networks, few studies allow for power and rate adaptation on spatial-temporal varying vehicle density in multiple neighboring road regions. Consequently, these existing optimization schemes may not provide optimal performance when applied to multi-region vehicular networks with limited resource blocks.

1.2 Motivation and Contributions

According to the 3GPP standard specification [1]–[3], [45], LTE-V2V networks exploit the single-carrier frequency-division multiple-access (SC-FDMA) protocol for their physical layer and MAC layer. The number of resource blocks in a signal frame is restricted and should be properly scheduled in response to varying vehicle density. Some analytical studies further show that vehicle density in the access environment significantly influences the reliability of LTE-V2V networks in Mode 3 [8]. Other studies [5], [6], [42] indicate that road traffic flows can significantly affect the data transmission rate of a vehicular network. However, to our knowledge, no existing studies have joined macroscopic traffic flow dynamics and MFD-based perimeter control into EE optimization of LTE-V2V networks. Therefore, this paper aims to fill the gap by developing a joint optimization framework. Our framework integrates multi-region MFD-based predictive perimeter traffic control and EE optimization of multi-region LTE-V2V networks. We differentiate our work from existing literature by enabling multi-region coordinated traffic dynamics-driven power control and beaconing rate adaptation for vehicular communications, providing new insight into multi-disciplinary modeling and optimization regarding communication and transportation.

We develop a hierarchical framework that jointly realizes MFD-based perimeter traffic flow control and power and beaconing rate optimization for LTE-V2V communications in multiple regions. Specifically, we propose a model predictive perimeter control integrated at the low level of the framework, which uses the MFDs of the multiple regions to predictively regulate the temporal-spatial dynamics of different traffic flows, including the internal and transfer flows in these regions. The low-level model predictive perimeter control aims to minimize the multi-region traffic network delays via dynamically controlling the transfer flows between adjacent regions. Moreover, we propose a communication optimization model at the high level, aiming to maximize the holistic EE performance of the multi-region LTE-V2V communication networks via jointly optimizing vehicular transmission power and broadcast beacon frequency. The high-level EE optimization model integrates the low-level MFD-based model predictive perimeter control and is driven by the multi-region regulated traffic flow dynamics. Thus, it adapts to the temporal-spatial evolution of vehicle density distributions over multi-region traffic networks. Our major contributions are summarized as follows.

(i) We theoretically derive the network connectivity in LTE-V2V communications based on the standard specification and further characterize the EE performance of LTE-V2V networks in multiple regions. The closed-form model explicitly considers the comprehensive effects of vehicular transmission power, broadcast beacon frequency, and multi-region traffic dynamics on EE performance.

(ii) We formulate a multi-region traffic flow dynamics model using the MFDs. We further propose a bi-objective joint optimization model integrating multi-region model predictive perimeter flow control with vehicular EE communication optimization. This joint optimization model leads to a hierarchical framework that enables the adaptive response of LTE-V2V communication networks to the temporal-spatial evolution of vehicle densities.

(iii) We also propose an iterative optimization method based on the augmented Lagrangian multiplier theory, which is integrated into the hierarchical framework for realizing joint optimization. The proposed method can transform constrained EE optimization into a sequence of unconstrained subproblems and exploits derivative-free opti-
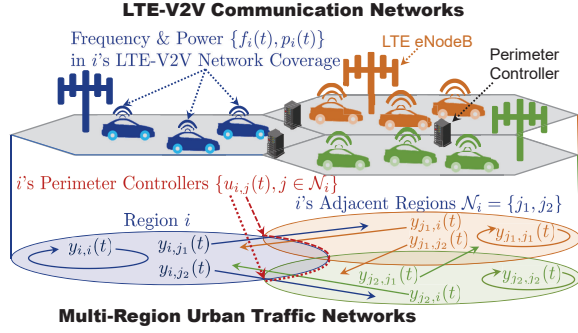
Fig. 1. An exemplary scenario of the intelligent transportation cyber-physical system in which the dynamics of vehicular communication networks and urban traffic networks are coupled.

mization techniques to tackle the non-smooth and strongly-nonlinear EE objective function. We prove the guaranteed convergence of the proposed optimization method.

1.3 Organization

We organize the rest of the paper as follows. Section 2 provides details about our hierarchical framework of joint EE communication optimization and model predictive perimeter control for multi-region LTE-V2V networks. Section 3 gives an algorithm design for solving the models. Section 4 provides simulation experiments for performance validation and comparison. Section 5 presents the main conclusion and remarks on our future work.

2 SYSTEM MODEL AND PROBLEM FORMULATION

As shown in Figure 1, we consider an application scenario in a city, where the entire urban traffic network is partitioned into several regions (or called cells). There exists at least a base station (or an Evolved NodeB (eNodeB)) for the coverage and service of the LTE radio access network in each urban region. Let $\mathcal{N} = \{1, 2, \ldots, N\}$ denote the set of the urban regions where N is the region number. In the scenario, the radio resource allocation in each region $i \in \mathcal{N}$ is operated by the LTE network in sidelink Mode 3 for supporting V2V applications (e.g., cooperative awareness) with the availability of cellular infrastructure.[1] The main symbols are summarized in Table 1.

2.1 Resources and Capacity of LTE-V2V Network

As specified by the LTE-V2V standard from 3GPP [2], the physical layer (PHY) and the medium access control (MAC) layer of the vehicular communication network employ the single-carrier frequency-division multiple access

---

1. In the urban scenario, LTE networks are almost ubiquitous nowadays. It is reasonable to consider that resource allocation is operated mainly in sidelink Mode 3 for connected vehicles [1], [3], [8]. For the case of sidelink Mode 4, some studies have already developed analytical models for performance evaluation in Mode 4, such as [9]. The different sidelink mode does not alter our methodology. As analytically analyzed in [9], traffic density (i.e., macroscopic traffic dynamics) significantly affects the resource allocation performance in Mode 4. Thus, these existing analytical models can be combined with our hierarchical framework to address more complicated resource allocation scenarios, which is left as our future work.

TABLE 1
Main Symbols and Definitions

Symbol	Definition
$\mathcal{N}$	set of urban regions
$m_{\text{RB}}^{\text{subframe}}$	RB number per subframe
$m_{\text{RB-PSSCH}}^{\text{subframe}}$	RB number per PSSCH subframe
L_{size}	beacon message size
I_{MCS}	index of a modulation and coding scheme
$m_{\text{RB}}^{\text{beacon}}(L_{\text{size}}, I_{\text{MCS}})$	RB number occupied by a beacon
$m_{\text{subframe}}^{\text{beacon}}(L_{\text{size}}, I_{\text{MCS}})$	subframe number occupied by a beacon
$\beta(L_{\text{size}}, I_{\text{MCS}})$	ratio of bandwidth occupation
f_i	beacon frequency used in region i
τ_{subframe}	duration of each subframe
$C_{\text{subframe}}^{\text{beacon}}(f_i)$	number of subframes per beacon period
$h(f_i; L_{\text{size}}, I_{\text{MCS}})$	number of vehicles for resource reuse
p_i	transmission power of vehicles in region i
d_l	distance associated with transmission link l
$g_{\text{LTE}}(d_l)$	channel gain associated with link l
$\boldsymbol{d}_{-l}$	distance set of l's interference links
$\gamma(p_i; d_l, \boldsymbol{d}_{-l})$	SINR associated with link l
$R(p_i)$	LTE-V2V resource reuse range in region i
λ_i	penetration rate of LTE-V2V vehicles in i
$x_i(t)$	vehicle accumulation in region i at time t
L_i	space-mean road length in region i
$\rho(x_i(t))$	LTE-V2V vehicle density in region i at t
$\Pr(m_i)$	probability of m_i vehicles occupying RBs
$\Pr(\text{outage}|m_i)$	outage probability conditioned on m_i
$q(x_i(t), f_i(t), p_i(t))$	outage probability of LTE-V2V network in i
$J_i(x_i(t), f_i(t), p_i(t))$	EE metric of LTE-V2V network in i
$\boldsymbol{x}(t), \boldsymbol{f}(t), \boldsymbol{p}(t)$	collections of $x_i(t)$, $f_i(t)$, and $p_i(t)$
$J(\boldsymbol{x}(t), \boldsymbol{f}(t), \boldsymbol{p}(t))$	total EE metric of multiple regions
$x_{i,j}(t)$	accumulation of vehicles from i to j at t
$g_i(x_i(t))$	MFD of region i depending on $x_i(t)$
$y_{i,j}(t)$	internal transfer flow from i to j at t
$Q_{i,j}(t)$	traffic demand generated from i to j at t
$u_{i,j}(t)$	perimeter flow controller between i and j
$\boldsymbol{u}(t)$	collection of $u_{i,j}(t)$
$W(\boldsymbol{u}(t))$	total vehicle accumulation of regions

(SC-FDMA). The SC-FDMA is a modified protocol of the well-known orthogonal frequency-division multiple access (OFDMA), which can reduce the peak-to-average power ratio (PAPR) and support multiple channels of 10 MHz or 20 MHz. In the time domain, the LTE-V2V communication technique organizes a wireless signal into several frames each with the duration of 10 ms, and each signal frame is usually divided into 10 subframes each with the duration of $\tau_{\text{subframe}} = 1$ ms. Each subframe further consists of two time slots. In the frequency domain, a wireless signal is modulated by a number of subcarriers each with the spacing of 15 kHz. Thus, the LTE-V2V communication network defines the smallest unit of the radio time-space resources allocated to vehicular users as a *Resource Block* (RB), and each RB contains 12 subcarriers (i.e., with the frequency wide of 12×15 kHz $= 180$ kHz) and one time slot of 1 ms/2 $= 0.5$ ms [3]. In the LTE-V2V communication network, a group of RBs in the same subframe can constitute a series of subchannels that are used to transmit vehicular

data and control information. That is, we can denote the number of the RBs per subframe by $m_{\text{RB}}^{\text{subframe}}$ and the typical RB amount per subframe in $10\,\text{MHz}$ channels is $m_{\text{RB}}^{\text{subframe}} = 100$. According to the standard specification [46], the RBs are exploited to realize three types of physical channels, among which the physical sidelink shared channels (PSSCH) are used to transmit application-specified data packets that are coded in a sequence of transport blocks (TBs), and the physical sidelink control channels (PSCCH) are used to transmit sidelink control information (SCI). In this paper, we consider the high-reliable and low-latency V2V communication application scenario based on periodically broadcasting beacons or cooperative awareness messages (CAM). An intact beacon or CAM can be packeted into one TB to be transmitted over the PSSCH. Thus, we mainly focus on the shared channels and denote the number of the RBs to be used for carrying the PSSCH per subframe by $m_{\text{RB-PSSCH}}^{\text{subframe}}$. A typical value of $m_{\text{RB-PSSCH}}^{\text{subframe}}$ in $10\,\text{MHz}$ channels is $m_{\text{RB-PSSCH}}^{\text{subframe}} = 81$ [8].

Additionally, according to the standard specification for the LTE-V2V communication [46], given a specific beacon or CAM size L_{size} and a specific modulation and coding scheme (MCS) I_{MCS}, the number of the RBs occupied by the shared channels used to transmit the packet is also determined. We can let $m_{\text{RB}}^{\text{beacon}}(L_{\text{size}}, I_{\text{MCS}})$ denote the number of the RBs allocated for a beacon that depends on the configurations L_{size} and I_{MCS}. Hence, we derive the number of the subframes occupied for transmitting a beacon, $m_{\text{subframe}}^{\text{beacon}}(L_{\text{size}}, I_{\text{MCS}})$, as follows

$$m_{\text{subframe}}^{\text{beacon}}(L_{\text{size}}, I_{\text{MCS}}) = \left\lceil \frac{m_{\text{RB}}^{\text{beacon}}(L_{\text{size}}, I_{\text{MCS}})}{m_{\text{RB-PSSCH}}^{\text{subframe}}} \right\rceil, \quad (1)$$

where $\lceil \cdot \rceil$ is the ceil function. Considering that the transmitted packets are uniformly allocated over the subchannels, we further estimate the ratio of the occupied bandwidth over the total available bandwidth, denoted by β, as follows

$$\beta(L_{\text{size}}, I_{\text{MCS}}) = \left\lceil \frac{m_{\text{RB}}^{\text{beacon}}(L_{\text{size}}, I_{\text{MCS}})}{m_{\text{subframe}}^{\text{beacon}}(L_{\text{size}}, I_{\text{MCS}})} \right\rceil \frac{1}{m_{\text{RB}}^{\text{subframe}}}. \quad (2)$$

On the other hand, let the beacon frequency of the LTE-V2V communication network in each urban region $i \in \mathcal{N}$ be f_i in Hz. The number of the allowed subframes per beacon period, i.e., the amount of the radio resources in the time domain, $C_{\text{subframe}}^{\text{beacon}}(f_i)$, is estimated by

$$C_{\text{subframe}}^{\text{beacon}}(f_i) = \left\lfloor \frac{T_i}{\tau_{\text{subframe}}} \right\rfloor, \quad i \in \mathcal{N}, \quad (3)$$

where T_i is the beacon period equal to $T_i = f_i^{-1}$ seconds and $\lfloor \cdot \rfloor$ is the floor function. Using (3) and (1), we can calculate the maximum allowed number of the LTE-V2V communication vehicles in a reciprocal resource reuse coverage that can be allocated without incurring any interference to each other during one beacon period, $h(f_i; L_{\text{size}}, I_{\text{MCS}})$, as follows

$$h(f_i; L_{\text{size}}, I_{\text{MCS}}) = \left\lfloor \frac{C_{\text{subframe}}^{\text{beacon}}(f_i)}{m_{\text{subframe}}^{\text{beacon}}(L_{\text{size}}, I_{\text{MCS}})} \right\rfloor, \quad i \in \mathcal{N}. \quad (4)$$

From (4), $h(f_i; L_{\text{size}}, I_{\text{MCS}})$ indicates the service capacity of the LTE-V2V communication network regarding its limited time-space radio resources, which not only relies on the network configurations L_{size} and I_{MCS} based on the standard specification but also the application-oriented design parameter (i.e., the beacon frequency) f_i. In general, increasing the beacon frequency f_i can increase the possibility of the destination nodes receiving the messages and update the received information more frequently, thus improving the application reliability and reducing the information dissemination latency to guarantee the quality of service (QoS). However, a larger beacon frequency will result in higher resource occupancy by each individual vehicle and more redundant messages in the network, thus reducing the tolerant number of the vehicles allocated per beacon period in the same resource reuse coverage $h(f_i; L_{\text{size}}, I_{\text{MCS}})$. Therefore, there is a tradeoff between the QoS performance of the LTE-V2V communication network and the adaption of the beacon frequency.

2.2 Connectivity and Network-Wide Energy Efficiency

To further estimate the outage probability of a LTE-V2V connection[2], we first analyze the effective LTE-V2V resource reuse range. Given a specific antenna gain g_0, a path loss factor at the reference distance of $1\,\text{m}$ L_0, and a path loss exponent α in the LTE-V2V communication scenario, we can typically evaluate the channel gain of a host LTE-V2V transmission link l, $g_{\text{LTE}}(d_l)$, as follows

$$g_{\text{LTE}}(d_l) = \frac{g_0}{L_0 d_l^\alpha}, \quad (5)$$

where d_l is the distance between the transmitter and the receiver of the host transmission link l.

Let the interfering node set associated with the LTE-V2V transmission link l in the urban region $i \in \mathcal{N}$ be $\mathcal{I}_l$ which consists of those transmitting nodes that can incur wireless interferences to the host transmission link l. The received instantaneous signal-to-noise-and-interference ratio (SINR) over the host transmission link l, $\gamma(p_i; d_l, \boldsymbol{d}_{-l})$, can be derived by

$$\gamma(p_i; d_l, \boldsymbol{d}_{-l}) = \frac{g_{\text{LTE}}(d_l)p_i}{\beta(L_{\text{size}}, I_{\text{MCS}})\sigma_i^2 + \sum_{v \in \mathcal{I}_l} g_{\text{LTE}}(d_v)p_i} \quad (6)$$

for $i \in \mathcal{N}$, where p_i is the transmission power of the LTE-V2V communication vehicles in the urban region i, d_v is the interference link distance associated with the v-th interference and $\boldsymbol{d}_{-l} = \text{col}\{d_v, v \in \mathcal{I}_l\}$. σ_i^2 is the background noise power in the region i. $\beta(L_{\text{size}}, I_{\text{MCS}})$ denotes the ratio of the utilized bandwidth over the total available bandwidth as defined in (2).

Given the minimum SINR level for correctly receiving and decoding signals from a transmitter, γ_{min}, and the cooperative awareness range for any vehicular application, R_0, the transmission power p_i, $i \in \mathcal{N}$, should always satisfy the minimum SINR level in an ideal situation where there exist no interferences, i.e., $\mathcal{I}_l = \emptyset$. At this point, we can get

$$\gamma_{\text{min}} \leq \frac{g_{\text{LTE}}(R_0)p_i}{\beta(L_{\text{size}}, I_{\text{MCS}})\sigma_i^2}. \quad (7)$$

---

2. In wireless communication, outage probability is a widely-used performance metric of a wireless communication system. It indicates the possibility that a receiver cannot receive the information from a transmitter correctly. In this work, the outage probability is specified as the probability that the LTE RBs cannot be allocated to a vehicle when all the RBs have already been allocated to others in the RB reuse range.

Combining (5) and (7), we can derive a lower bound for the feasible transmission power design in the region i, denoted by p_i^-, as follows

$$p_i \geq p_i^- = \frac{\gamma_{\min}\beta\left(L_{\text{size}}, I_{\text{MCS}}\right)\sigma_i^2 L_0 R_0^\alpha}{g_0}. \tag{8}$$

Let $R(p_i)$ denote the LTE-V2V resource reuse range in the urban region $i \in \mathcal{N}$ that depends on the adopted transmission power p_i. Generally, any an interfering node located at the distance of $R(p_i)$ from the transmitter of the host transmission link l will not impair the host transmission link if the SINR of the host transmission link is not smaller than the minimum level $\gamma_{\min}$. To derive the closed-form design of $R(p_i)$, we suppose that the transmitter of the host transmission link l is exactly located at the distance of R_0 from its receiver and an interfering node is at the distance of $R(p_i)$ from the transmitter of the host transmission link l. Thus, the worst-case SINR is attained when the interfering node is also located in the same direction as that of the receiver. At this point, we have

$$\gamma_{\min} \leq \frac{g_{\text{LTE}}(R_0)p_i}{\beta\left(L_{\text{size}}, I_{\text{MCS}}\right)\sigma_i^2 + g_{\text{LTE}}\left(R(p_i) - R_0\right)p_i}, \tag{9}$$

which further leads to

$$R(p_i) - R_0 \geq R_0\left(\frac{1}{\gamma_{\min}} - \frac{\beta\left(L_{\text{size}}, I_{\text{MCS}}\right)\sigma_i^2 L_0 R_0^\alpha}{p_i g_0}\right)^{-\frac{1}{\alpha}}. \tag{10}$$

On the other side, the distance between the interfering node and the receiver of the host transmission link l should be larger than that of the host transmission link, i.e., R_0. Thus, we can also have

$$R(p_i) - R_0 \geq R_0. \tag{11}$$

Combining (10) and (11), we can derive the LTE-V2V resource reuse range $R(p_i)$ as

$$R(p_i) = \Delta R + R_0$$
$$+ R_0 \max\left\{\left(\frac{1}{\gamma_{\min}} - \frac{\beta\left(L_{\text{size}}, I_{\text{MCS}}\right)\sigma_i^2 L_0 R_0^\alpha}{p_i g_0}\right)^{-\frac{1}{\alpha}}, 1\right\}, \tag{12}$$

where ΔR is a constant margin that is introduced when considering the existence of vehicle positioning errors in an actual LTE-V2V network. That is, as suggested by the 3GPP specification [47], [48], the LTE-V2V network relies on the time difference of arrival (TDOA) of the uplinks to approximately estimate the vehicle positions, which inevitably introduces measure errors. Thus, the resource reuse range should take into consideration a certain margin ΔR to deal with such location errors. For instance, according to the technical report [49], the uplink TDOA measurements with the assistance of five eNodeBs can achieve the position detection accuracy of about 100 meters under the sensing-based SPS scheme. Hence, a typical settings on ΔR can be specified as $\Delta R = 100\,\text{m}$.

Let $x_i(t)$ (veh) denote the vehicle accumulation in the region $i \in \mathcal{N}$ at time $t \in \mathbb{R}_{\geq 0}$ and λ_i denote the space-mean penetration rate of the LTE-V2V communications in the same region. The average density of the LTE-V2V communication vehicles in $i \in \mathcal{N}$ is denoted by $\rho(x_i(t))$, i.e.,

$$\rho(x_i(t)) = \frac{\lambda_i x_i(t)}{L_i},\ i \in \mathcal{N}, \tag{13}$$

where L_i represents the average (space-mean) road length of the road network in the urban region i. Besides, within each urban region, we consider that the spatial distribution of the LTE-V2V communication vehicles follows an independent homogeneous Poisson Point Process (PPP) characterized by the parameter $\rho(x_i(t))$ as indicated by the current literature [50]–[52]. Therefore, we can derive the probability that there exist m_i LTE-V2V communication vehicles allocated with the RBs in the resource reuse range $R(p_i)$ in the region i as

$$\Pr(m_i) = \frac{\left[\rho(x_i(t))R(p_i)\right]^{m_i}e^{-\rho(x_i(t))R(p_i)}}{m_i!},i \in \mathcal{N}. \tag{14}$$

Under the condition that there already are m_i vehicles allocated with the RBs in the LTE-V2V resource reuse range $R(p_i)$ in the region i, the outage probability of the network is the possibility that the number of the LTE-V2V communication vehicles exceeds the number of the LTE-V2V resources. Recalling (4), the conditional outage probability is formulated as the fraction of those LTE-V2V communication vehicles exceeding the maximum allowed number in the resource reuse range, i.e.,

$$\Pr(\text{outage}|m_i)$$
$$= \frac{m_i - h(f_i; L_{\text{size}}, I_{\text{MCS}})}{m_i}1_{m_i-h(f_i;L_{\text{size}},I_{\text{MCS}})\geq 0} \tag{15}$$

for all $i \in \mathcal{N}$, where $1_{m_i-h(f_i;L_{\text{size}},I_{\text{MCS}})\geq 0}$ is a binary indicator that is equal to 1 if and only if $m_i - h(f_i; L_{\text{size}}, I_{\text{MCS}}) \geq 0$ holds, otherwise 0. Combining (14) and (15), we can derive the total outage probability of the LTE-V2V communication network, denoted by $q(x_i(t), f_i(t), p_i(t))$, as follows

$$q(x_i(t), f_i(t), p_i(t)) =$$
$$\sum_{m_i=h(f_i(t);L_{\text{size}},I_{\text{MCS}})+1}^{\infty} \Pr(\text{outage}|m_i)\Pr(m_i) \tag{16}$$

for all $i \in \mathcal{N}$. Here, we introduce t for p_i and f_i, and use $p_i(t)$ and $f_i(t)$ to equivalently represent p_i and f_i, respectively, in order to emphasize their time dependence.

Substituting (14) and (15) into (16), we can further get a closed-form approximation on the outage probability as

$$q(x_i(t), f_i(t), p_i(t)) =$$
$$[\rho(x_i(t))R(p_i(t))]^{h(f_i(t);L_{\text{size}},I_{\text{MCS}})+1}e^{-\rho(x_i(t))R(p_i(t))}\times$$
$$\sum_{k=0}^{\infty}\frac{k+1}{[h(f_i(t);L_{\text{size}},I_{\text{MCS}})+1+k]}\frac{[\rho(x_i(t))R(p_i(t))]^k}{[h(f_i(t);L_{\text{size}},I_{\text{MCS}})+1+k]!}$$
$$= \frac{[\rho(x_i(t))R(p_i(t))]^{h(f_i(t);L_{\text{size}},I_{\text{MCS}})+1}e^{-\rho(x_i(t))R(p_i(t))}}{[h(f_i(t);L_{\text{size}},I_{\text{MCS}})+1][h(f_i(t);L_{\text{size}},I_{\text{MCS}})+1]!}\times$$
$$\sum_{k=0}^{\infty}\frac{(2)_k(h(f_i(t);L_{\text{size}},I_{\text{MCS}})+1)_k}{[(h(f_i(t);L_{\text{size}},I_{\text{MCS}})+2)_k]^2}\frac{[\rho(x_i(t))R(p_i(t))]^k}{k!} \tag{17}$$

where $(a)_k$ is the Pochhammer's symbol that denotes the product $(a)_k = a(a+1)\cdots(a+k-1)$. According to the theory of generalized hypergeometric series, we can formally represent the summation term in (17) by using

a specific Generalized Hypergeometric Function (GHF) as follows

$$
{}_2F_2\left(\begin{matrix} 2 & h_{i,t}+1 \\ h_{i,t}+2 & h_{i,t}+2 \end{matrix}; \rho_{i,t}\right) = \sum_{k=0}^{\infty} \frac{(2)_k\,(h_{i,t}+1)_k}{\left[(h_{i,t}+2)_k\right]^2}\frac{\rho_{i,t}^k}{k!}
\tag{18}
$$

with $\rho_{i,t} = \rho\left(x_i(t)\right)R\left(p_i(t)\right)$ and $h_{i,t} = h\left(f_i(t); L_{\text{size}}, I_{\text{MCS}}\right)$ for notional simplicity for all $i \in \mathcal{N}$. Using (18), we can derive the formal representation for the outage probability $q\left(x_i(t), f_i(t), p_i(t)\right)$ as

$$
\begin{aligned}
&q\left(x_i(t), f_i(t), p_i(t)\right) \\
&= \frac{\rho_{i,t}^{h_{i,t}+1}e^{-\rho_{i,t}}}{(h_{i,t}+1)\,(h_{i,t}+1)!}{}_2F_2\left(\begin{matrix} 2 & h_{i,t}+1 \\ h_{i,t}+2 & h_{i,t}+2 \end{matrix}; \rho_{i,t}\right)
\end{aligned}
\tag{19}
$$

for all $i \in \mathcal{N}$.

From (19), the average connectivity can be estimated as $1 - q\left(x_i(t), f_i(t), p_i(t)\right)$. Thus, we formulate the EE metric in each urban region as the average data rate achieved per power consumption, i.e.,

$$
J_i\left(x_i(t), f_i(t), p_i(t)\right) = \frac{\left[1 - q\left(x_i(t), f_i(t), p_i(t)\right)\right]f_i(t)L_{\text{size}}}{p_i(t)}.
\tag{20}
$$

It is noted that the EE metric in (20) reflects the amount of the data bits that can be transmitted by consuming one unit of energy. Based on (20), the network-wide energy efficiency is then defined by summing up the EE of all the urban regions as follows

$$
J\left(\boldsymbol{x}(t), \boldsymbol{f}(t), \boldsymbol{p}(t)\right) = \sum_{i \in \mathcal{N}} J_i\left(x_i(t), f_i(t), p_i(t)\right),
\tag{21}
$$

where $\boldsymbol{x}(t)$, $\boldsymbol{f}(t)$ and $\boldsymbol{p}(t)$ are the collections of the accumulation states, the broadcast frequencies, and the transmission power levels in the whole regions, respectively, i.e., $\boldsymbol{x}(t) = \text{col}\{x_i(t), i \in \mathcal{N}\}$, $\boldsymbol{f}(t) = \text{col}\{f_i(t), i \in \mathcal{N}\}$, and $\boldsymbol{p}(t) = \text{col}\{p_i(t), i \in \mathcal{N}\}$. It is observed from (21) that the evaluation of the network-wide energy efficiency $J\left(\boldsymbol{x}(t), \boldsymbol{f}(t), \boldsymbol{p}(t)\right)$ relies on the spatial time-varying vehicle density $\rho\left(x_i(t)\right)$. The optimization of $J\left(\boldsymbol{x}(t), \boldsymbol{f}(t), \boldsymbol{p}(t)\right)$ requires modeling the macroscopic traffic flow dynamics, which is detailed in the following section.

2.3 Evolution Dynamics of Spatial Vehicle Density

In transportation science, the MFD of different urban regions describes the relationship between the vehicle density of the road traffic network and the regions' outflow or the network's space-mean flow [21], [23]. This theoretical tool connects the vehicle accumulation in a region to the output flow of the region, providing a fundamental for developing different perimeter flow controllers. Perimeter control is a typical kind of macroscopic traffic control, which aims to regulate the traffic flows transferring at the perimeter border of two neighboring regions [10]. Therefore, to model the aggregate traffic flow dynamics in the entire urban network and derive the evolution dynamics of the spatial vehicle density in each urban region, we use the macroscopic traffic modeling approach based on the MFD and exploit the MFD-based perimeter flow control.

For the urban regions $i \in \mathcal{N}$, we further let $x_{i,j}(t)$ be the accumulation of vehicles in the region i with the region j as

their destination at time t, and $Q_{i,j}(t)$ be the traffic demand flow generated in the region i with the destination region j at t, i, $j \in \mathcal{N}$. We also denote the set of the urban regions adjacent to i by $\mathcal{N}_i$, i.e., $\mathcal{N} = \cup_{i=1}^{N}\mathcal{N}_i$. Accordingly, we can calculate the total vehicle accumulation in each region by

$$
x_i(t) = x_{i,i}(t) + \sum_{j \in \mathcal{N}_i} x_{i,j}(t), \ i \in \mathcal{N}.
\tag{22}
$$

Moreover, for each urban region $i \in \mathcal{N}$, we consider that there admits a well-defined MFD, denoted by $g_i\left(x_i(t)\right)$ (veh/s), that captures the outflow dynamics (trip completion flow) at accumulation $x_i(t)$. The consideration is exactly in line with many current studies [10]–[14], [21], [53]–[62]. The MFD here describes a macroscopic similarity that all the trips within a region have similar trip lengths at an aggregate level, i.e., the travel distance of each vehicle inside a region is approximately independent of the origin and destination of its trip. According to the simulation and empirical study [23], the MFD shape can be well approximated by a non-symmetric unimodal curve skewed to the right (i.e., there exists a critical density maximizing $g_i\left(x_i(t)\right)$ and this critical density is smaller than the half of the jam accumulation at which the network is blocked). This allows us to adopt a third-order polynomial with respect to $x_i(t)$ to represent $g_i\left(x_i(t)\right)$ as follows

$$
g_i\left(x_i(t)\right) = \sum_{v=0}^{3} a_{i,v}\left[x_i(t)\right]^v, \ i \in \mathcal{N},
\tag{23}
$$

where $a_{i,3} \neq 0$ and $a_{i,v}$ ($v \in \{0, 1, \ldots, 3\}$, $i \in \mathcal{N}$) are the polynomial coefficients that can be estimated from historical traffic data in practice [10], [21], [24], [25], [60]. Here, it is remarked that the MFD properties regarding the traffic heterogeneity and different cases of trip patterns inside a region have also been investigated and can be found in [10], [24], [25]. Other alternative forms of the MFD will not alter our proposed methodological approach in this work.

Let $y_{i,i}(t)$ denote the internal transfer flow in the region i at time t, and $y_{i,j}(t)$ be the external transfer flow from i to j at t. Using the MFDs, we can obtain the internal and the external transfer flows as follows

$$
\begin{cases}
y_{i,i}(t) = \dfrac{x_{i,i}(t)}{x_i(t)}g_i\left(x_i(t)\right), \\[2mm]
y_{i,j}(t) = \dfrac{x_{i,j}(t)}{x_i(t)}g_i\left(x_i(t)\right),
\end{cases}
\tag{24}
$$

for all $i \neq j$ and $i, j \in \mathcal{N}$. Now, we introduce the time-varying control variables $u_{i,j}(t)$ and $u_{j,i}(t)$, $u_{i,j}(t), u_{j,i}(t) \in [0, 1]$ for all $i \in \mathcal{N}$ and $j \in \mathcal{N}_i$, to represent the perimeter controllers existing between any two regions i and j. These perimeter controllers aim to regulate the transfer flows between any two adjacent regions. It is also noted that since each perimeter controller is only deployed on the border between two regions, it does not impact the internal traffic flows inside the regions. That is, the perimeter controllers are used to regulate $y_{i,j}(t)$ for any $i \neq j$ rather than $y_{i,i}(t)$ for all $i \in \mathcal{N}$. Consequently, following the mass conservation principle, we obtain a group of ordinary differential

equations (ODE) to describe the traffic flow dynamics of the multi-region MFD-based system as follows

$$
\begin{cases}
\dfrac{dx_{i,i}(t)}{dt} = Q_{i,i}(t) - y_{i,i}(t) + \displaystyle\sum_{j \in \mathcal{N}_i} u_{j,i}(t)y_{j,i}(t), \\
\dfrac{dx_{i,j}(t)}{dt} = Q_{i,j}(t) - \displaystyle\sum_{j \in \mathcal{N}_i} u_{i,j}(t)y_{i,j}(t),
\end{cases} \tag{25}
$$

for all $j \in \mathcal{N}_i$ and $i \in \mathcal{N}$.

2.4 Joint Optimization Framework

We aim to optimize vehicular communication and the urban traffic network. For this goal, we develop a joint optimization framework based on the model predictive control (MPC) approach. It has a bi-level structure that minimizes the total traffic delay of all the urban regions by manipulating the perimeter controllers, meanwhile maximizing the EE performance of LTE-V2V communications by adapting both vehicular transmission power and beacon rate to the macroscopic traffic dynamics in these regions.[3]

Specifically, let the initial time for the prediction horizon of the MPC-based perimeter controllers be t_c and the terminal time be t_f. We consider the prediction horizon as $t \in [t_c, t_f]$. The vehicle accumulation at t_c for $i, j \in \mathcal{N}$ is $x_{i,j}(t_c)$, which is known as the initial condition for the dynamics model (25). Without loss of generality, we use the symbols a^- and a^+ to denote the lower and the upper bounds of a, respectively. Hence, the lower and the upper bounds of the perimeter controllers $u_{i,j}(t)$ are $u_{i,j}^- \geq 0$ and $u_{i,j}^+ \leq 1$, respectively, i.e., $u_{i,j}(t) \in \left[u_{i,j}^-, u_{i,j}^+\right] \subseteq [0, 1]$. A lower bound of the total accumulation with respect to the region $i \in \mathcal{N}$ is denoted by $x_i^- \geq 0$. The jam accumulation for $i \in \mathcal{N}$ is x_i^+, which is treated as the upper bound of the accumulation $x_i(t)$. Thus, we have $x_i(t) \in [x_i^-, x_i^+]$. Similarly, the lower and the upper bounds of $x_{i,j}(t)$, $i, j \in \mathcal{N}$, are represented by $x_{i,j}^- \geq 0$ and $x_{i,j}^+ \leq x_i^+$, respectively, i.e., $x_{i,j}(t) \in \left[x_{i,j}^-, x_{i,j}^+\right] \subseteq [x_i^-, x_i^+]$.

Besides, for notational simplicity, we define the overall accumulation of all the urban regions by $W(\boldsymbol{u}(t))$ where $\boldsymbol{u}(t) = \{u_{i,j}(t), j \in \mathcal{N}_i, i \in \mathcal{N}\}$, i.e., letting

$$
W(\boldsymbol{u}(t)) = \sum_{i \in \mathcal{N}} x_{i,i}(t) + \sum_{i \in \mathcal{N}} \sum_{j \in \mathcal{N}_i} x_{i,j}(t). \tag{26}
$$

Given a set of the perimeter control inputs $\{\boldsymbol{u}(t), t \in [t_c, t_f]\}$, we can obtain the total vehicle accumulations of all the urban regions by using (25) and (22) correspondingly, $\{\boldsymbol{x}(t), t \in [t_c, t_f]\}$. Thus, we can denote such a mapping from $\{\boldsymbol{u}(t), t \in [t_c, t_f]\}$ to $\{\boldsymbol{x}(t), t \in [t_c, t_f]\}$ be $\mathcal{T}$, i.e., $\mathcal{T} : \boldsymbol{u}(t) \to \boldsymbol{x}(t), \forall t \in [t_c, t_f]$. The overall joint optimization

---

3. In transportation science, the total delay of a road traffic network is defined as the integral of the multiple regions' road traffic accumulation with respect to time [10], [21], [63].

---

problem is formulated as a bi-level constrained nonlinear programming model

$$
\begin{aligned}
&\max_{\boldsymbol{f}(t), \boldsymbol{p}(t), t \in [t_c, t_f]} : \int_{t_c}^{t_f} J\left(\mathcal{T}(\boldsymbol{u}(t)), \boldsymbol{f}(t), \boldsymbol{p}(t)\right) dt \\
&\min_{\boldsymbol{u}(t), t \in [t_c, t_f]} : \int_{t_c}^{t_f} W(\boldsymbol{u}(t)) dt \\
&\text{s.t.} : \begin{cases}
f_i^- \leq f_i(t) \leq f_i^+, \ i \in \mathcal{N}; \\
p_i^- \leq p_i(t) \leq p_i^+, \ i \in \mathcal{N}; \\
u_{i,j}^- \leq u_{i,j}(t) \leq u_{i,j}^+, \ j \in \mathcal{N}_i, \ i \in \mathcal{N}; \\
x_{i,j}^- \leq x_{i,j}(t) \leq x_{i,j}^+, \ i, \ j \in \mathcal{N}; \\
x_i^- \leq x_i(t) \leq x_i^+, \ i \in \mathcal{N}; \\
(21) - (26), \ t \in [t_c, t_f].
\end{cases}
\end{aligned} \tag{27}
$$

3 OPTIMIZATION ALGORITHM DESIGN

It is difficult to directly solve an optimal global solution of the multi-objective optimization problem (27). We resort to Pareto optimality for joint vehicular communication optimization and macroscopic traffic control (VCOMTC). Therefore, we turn to solve a Pareto-optimal solution. A feasible solution for (27) is considered Pareto optimal if and only if no other feasible solution exists that can improve the quality of any of the model's objective criteria without deteriorating at least one other objective criterion. Accordingly, letting $P_1(\boldsymbol{X}) = -\int_{t_c}^{t_f} J\left(\mathcal{T}(\boldsymbol{u}(t)), \boldsymbol{f}(t), \boldsymbol{p}(t)\right) dt$ and $P_2(\boldsymbol{X}) = \int_{t_c}^{t_f} W(\boldsymbol{u}(t)) dt$ denote the two optimization objectives in (27), respectively, where $\boldsymbol{X} = \{\boldsymbol{u}(t), \boldsymbol{f}(t), \boldsymbol{p}(t), t \in [t_c, t_f]\}$ represents a feasible solution of (27), we introduce the concept of Pareto-optimal feasible communication and control solution as follows:

Definition 1 (Pareto-optimal feasible solution). A feasible solution $\boldsymbol{X}^*$ for (27) is non-dominated or Pareto optimal if the following holds for any other feasible solution $\boldsymbol{X}$ of (27), $\boldsymbol{X} \neq \boldsymbol{X}^*$,

$$
\begin{cases}
P_l(\boldsymbol{X}^*) \leq P_l(\boldsymbol{X}), \ \forall l \in \{1, 2\}; \\
P_{l'}(\boldsymbol{X}^*) < P_{l'}(\boldsymbol{X}), \ \exists l' \in \{1, 2\}.
\end{cases} \tag{28}
$$

When carefully looking into (27), the LTE-V2V communication optimization-oriented decision variables $\boldsymbol{f}(t)$ and $\boldsymbol{p}(t)$ are decoupled with the optimal control objective of the multi-region urban traffic network, $P_2(\boldsymbol{X})$. Thus, this motivates us to decompose the multiple objective optimization problem into two sub-problems so as to obtain a Pareto-optimal feasible solution. One of the sub-problem is a high-level nonlinear constrained optimization sub-problem with respect to the LTE-V2V communications and the other is a low-level model predictive perimeter control with the MFD. Besides, to make the problem tractable, we also discretize the overall problem by dividing the prediction horizon into K_p time steps each with the duration of ΔT seconds, i.e., letting $t_f - t_c = K_p \Delta T$. The set of step indexes for the perimeter control inputs is denoted by the set of the finite prediction steps $\mathcal{K} = \{0, 1, \ldots, K_p - 1\}$.

3.1 The Low-Level Model Predictive Perimeter Control

For the low-level sub-problem, we denote the state and control vectors by $\boldsymbol{x}(k) = \mathrm{col}\{x_{i,j}(k), i, j \in \mathcal{N}\}$ and $\boldsymbol{u}(k) = \mathrm{col}\{u_{i,j}(k), j \in \mathcal{N}_i, i \in \mathcal{N}\}$. We define a state function by $F_{i,j}(\boldsymbol{x}(k), \boldsymbol{u}(k)), i, j \in \mathcal{N}$, as follows

$$
F_{i,j}(\boldsymbol{x}(k), \boldsymbol{u}(k)) =
\begin{cases}
Q_{i,i}(k) - y_{i,i}(k) + \displaystyle\sum_{v \in \mathcal{N}_i} u_{v,i}(k) y_{v,i}(k), j = i; \\
Q_{i,j}(k) - \displaystyle\sum_{v \in \mathcal{N}_i} u_{i,v}(k) y_{i,v}(k), j \in \mathcal{N}_i; \\
0, j \notin \mathcal{N}_i, j \neq i.
\end{cases}
\tag{29}
$$

Then, we derive the time-discrete MPC-based perimeter control model as

$$
\min_{\boldsymbol{u}(k), k \in \mathcal{K}} : C(\mathcal{U}) = \sum_{k \in \mathcal{K}} W(\boldsymbol{u}(k)) \Delta T
$$

$$
\text{s.t.} \begin{cases}
x_{i,j}(k+1) = x_{i,j}(k) + F_{i,j}(\boldsymbol{x}(k), \boldsymbol{u}(k)) \Delta T, i, j \in \mathcal{N}; \\
u_{i,j}^- \leq u_{i,j}(k) \leq u_{i,j}^+, j \in \mathcal{N}_i, i \in \mathcal{N}; \\
x_{i,j}^- \leq x_{i,j}(k) \leq x_{i,j}^+, i, j \in \mathcal{N}; \\
x_i^- \leq x_i(k) \leq x_i^+, i \in \mathcal{N}; \\
k \in \mathcal{K}.
\end{cases}
\tag{30}
$$

Here, (30) presents an open-loop time-discrete MPC model for determining the optimal perimeter control of the multi-region urban network. Similar to the current literature [10], [11], [14], [21], [57], [60], the MPC model with the MFD can be solved by exploiting some well-known numerical optimal control toolboxes integrating nonlinear programming solvers, such as GPOPS-II (Next-Generation Optimal Control Software) [64], MPT (Multi-Parametric Toolbox) [65], and MATLAB MPC toolbox [66]. Let $\mathcal{U}^*$ denote the set of the optimal perimeter control inputs obtained by solving (30), i.e., $\mathcal{U}^* = \mathrm{col}\{\boldsymbol{u}^*(k), k \in \mathcal{K}\}$ and $\boldsymbol{u}^*(k) = \mathrm{col}\{u_{i,j}^*(k), j \in \mathcal{N}_i, i \in \mathcal{N}\}$ where $u_{i,j}^*(k)$ is the optimal perimeter control input for the boundary between two adjacent regions i and j at k. The optimal vehicle accumulations of the urban regions can also be determined by $\boldsymbol{x}^*(t) = \mathcal{T}(\boldsymbol{u}^*(t))$ for all $k \in \mathcal{K}$.

3.2 The High-Level Communication Optimization

For the high-level sub-problem, we can formulate the time-discrete nonlinear constrained optimization model to obtain the jointly-optimal beacon frequency and transmission power of the LTE-V2V communication vehicles, denoted by $\mathcal{F}^* = \mathrm{col}\{\boldsymbol{f}^*(k), k \in \mathcal{K}\}$ and $\mathcal{P}^* = \mathrm{col}\{\boldsymbol{p}^*(k), k \in \mathcal{K}\}$, respectively, where $\boldsymbol{f}^*(k)$ and $\boldsymbol{p}^*(k)$ are the optimal beacon frequency and transmission power, respectively. This high-level optimization model is driven by the optimal perimeter control $\mathcal{U}^*$ of the multi-region urban traffic network obtained from the low-level model, i.e., treating $\boldsymbol{x}^*(t) = \mathcal{T}(\boldsymbol{u}^*(t))$ for $\boldsymbol{u}^*(t) \in \mathcal{U}^*$ as the inputs of the high-level model. Specifically, from (27), the high-level time-

discrete nonlinear constrained optimization model driven by $\boldsymbol{x}^*(t) = \mathcal{T}(\boldsymbol{u}^*(k)), \boldsymbol{u}^*(k) \in \mathcal{U}^*$, is formulated as follows

$$
\min_{\mathcal{F}, \mathcal{P}} : V(\mathcal{F}, \mathcal{P}) = -\sum_{k \in \mathcal{K}} J(\mathcal{T}(\boldsymbol{u}^*(k)), \boldsymbol{f}(k), \boldsymbol{p}(k)) \Delta T
$$

$$
\text{s.t.} : \begin{cases}
f_i^- \leq f_i(k) \leq f_i^+, i \in \mathcal{N}; \\
p_i^- \leq p_i(k) \leq p_i^+, i \in \mathcal{N}; \\
\boldsymbol{u}^*(k) \in \mathcal{U}^*, \forall k \in \mathcal{K}.
\end{cases}
\tag{31}
$$

where $\mathcal{F} = \mathrm{col}\{\boldsymbol{f}(k), k \in \mathcal{K}\}$ and $\mathcal{P} = \mathrm{col}\{\boldsymbol{p}(k), k \in \mathcal{K}\}$.

To proceed, we propose an optimization approach by combining the unconstrained optimization and the derivative-free optimization techniques, which does not require any information about the gradient or the Hessian matrix of the non-smooth objective function $V(\mathcal{F}, \mathcal{P})$ with respect to $\mathcal{F}$ and $\mathcal{P}$. The underlying idea for solving the non-smooth (31) is to transform it into an unconstrained problem and then enable the derivative-free unconstrained optimization technique to come into play.

To be specific, we introduce a set of nonnegative slack variables, $\mathcal{Z} = \mathrm{col}\left\{z_{l,i}^2(k), l = 1, \ldots, 4; i \in \mathcal{N}; k \in \mathcal{K}\right\}$, and let $\mu_{1,i}(k) = f_i(k) - f_i^-$, $\mu_{2,i}(k) = f_i^+ - f_i(k)$, $\mu_{3,i}(k) = p_i(k) - p_i^-$ and $\mu_{4,i}(k) = p_i^+ - p_i(k)$ for all $i \in \mathcal{N}$ and $k \in \mathcal{K}$, such that those inequality constraints of (31) are equivalently transformed into the equalities as follows

$$
\min_{\mathcal{F}, \mathcal{P}, \mathcal{Z}} : V(\mathcal{F}, \mathcal{P}) = -\sum_{k \in \mathcal{K}} J(\mathcal{T}(\boldsymbol{u}^*(k)), \boldsymbol{f}(k), \boldsymbol{p}(k)) \Delta T
$$

$$
\text{s.t.} : \begin{cases}
\mu_{l,i}(k) - z_{l,i}^2(k) = 0, 1 = 1, \ldots, 4; i \in \mathcal{N}; \\
\boldsymbol{u}^*(k) \in \mathcal{U}^*, \forall k \in \mathcal{K}.
\end{cases}
\tag{32}
$$

Following (32), we derive the augmented Lagrangian function $\widetilde{\mathcal{L}}_\sigma(\mathcal{F}, \mathcal{P}, \mathcal{Z}, \boldsymbol{\lambda})$ with a column of the Lagrange multipliers $\boldsymbol{\lambda} = \mathrm{col}\{\lambda_{l,i}(k) \in \mathbb{R}, l = 1, \ldots, 4; i \in \mathcal{N}; k \in \mathcal{K}\}$ and a positive penalty factor $\sigma > 0$ as follows

$$
\begin{aligned}
\widetilde{\mathcal{L}}_\sigma(\mathcal{F}, \mathcal{P}, \mathcal{Z}, \boldsymbol{\lambda}) =& V(\mathcal{F}, \mathcal{P}) \\
& - \sum_{k \in \mathcal{K}} \sum_{i \in \mathcal{N}} \sum_{l=1}^4 \lambda_{l,i}(k) \left[\mu_{l,i}(k) - z_{1,i}^2(k)\right] \\
& + \frac{\sigma}{2} \sum_{k \in \mathcal{K}} \sum_{i \in \mathcal{N}} \sum_{l=1}^4 \left[\mu_{l,i}(k) - z_{1,i}^2(k)\right]^2.
\end{aligned}
\tag{33}
$$

Based on (33), we can obtain the following result:

Lemma 1. The optimization of $\widetilde{\mathcal{L}}_\sigma(\mathcal{F}, \mathcal{P}, \mathcal{Z}, \boldsymbol{\lambda})$ is equivalent to the optimization of $\mathcal{L}_\sigma(\mathcal{F}, \mathcal{P}, \boldsymbol{\lambda})$ where $\mathcal{L}_\sigma(\mathcal{F}, \mathcal{P}, \boldsymbol{\lambda})$ is given as

$$
\begin{aligned}
\mathcal{L}_\sigma(\mathcal{F}, \mathcal{P}, \boldsymbol{\lambda}) =& V(\mathcal{F}, \mathcal{P}) \\
& + \frac{1}{2\sigma} \sum_{k \in \mathcal{K}} \sum_{i \in \mathcal{N}} \sum_{l=1}^4 \left\{\psi_{l,i}^2(k) - \lambda_{l,i}^2(k)\right\}
\end{aligned}
\tag{34}
$$

and $\psi_{l,i}(k)$ is given as

$$
\psi_{l,i}(k) = \begin{cases}
\lambda_{l,i}(k) - \sigma \mu_{l,i}(k), \lambda_{l,i}(k) \geq \sigma \mu_{l,i}(k); \\
0, \text{ otherwise.}
\end{cases}
\tag{35}
$$

The proof of Lemma 1, which is omitted here for the sake of saving space, is provided in Appendix B in the supplementary material. To proceed, we provide another lemma based on the matrix theory as follows . The proof of Lemma 2 is also detailed in Appendix C in the supplementary material.

Lemma 2. Given matrices $\boldsymbol{A} \in \mathbb{R}^{n \times n}$ and $\boldsymbol{B} \in \mathbb{R}^{n \times m}$, the strict inequality $\boldsymbol{x}^{\mathrm{T}} \boldsymbol{A} \boldsymbol{x} > 0$ always holds true for any non-zero column vector $\boldsymbol{x} \neq \boldsymbol{0}$, $\boldsymbol{x} \in \mathbb{R}^{n \times 1}$, satisfying $\boldsymbol{B}^{\mathrm{T}} \boldsymbol{x} = \boldsymbol{0}$, if and only if there exists a positive constant $\sigma^* > 0$, such that $\boldsymbol{x}^{\mathrm{T}}(\boldsymbol{A} + \sigma \boldsymbol{B} \boldsymbol{B}^{\mathrm{T}}) \boldsymbol{x} > 0$ always holds true for any $\sigma \geq \sigma^*$.

For the simplicity of notations, let $\phi_{l,i}(k) = \mu_{l,i}(k) - z_{l,i}^2(k)$ for all $l = 1, \ldots, 4$, $i \in \mathcal{N}$, and $k \in \mathcal{K}$. The Lagrangian function of (32) can be expressed as follows

$$
\widetilde{\mathcal{L}}(\mathcal{F}, \mathcal{P}, \mathcal{Z}, \boldsymbol{\lambda}) = V(\mathcal{F}, \mathcal{P}) - \sum_{k \in \mathcal{K}} \sum_{i \in \mathcal{N}} \sum_{l=1}^{4} \lambda_{l,i}(k) \phi_{l,i}(k),
\tag{36}
$$

and the augmented one in (33) is re-arranged as

$$
\widetilde{\mathcal{L}}_{\sigma}(\mathcal{F}, \mathcal{P}, \mathcal{Z}, \boldsymbol{\lambda}) = \widetilde{\mathcal{L}}(\mathcal{F}, \mathcal{P}, \mathcal{Z}, \boldsymbol{\lambda}) + \frac{\sigma}{2} \sum_{k \in \mathcal{K}} \sum_{i \in \mathcal{N}} \sum_{l=1}^{4} \phi_{l,i}^2(k).
\tag{37}
$$

Since the objective function $V(\mathcal{F}, \mathcal{P})$ is non-smooth within its feasible domain, there exist some finite feasible points, i.e., some feasible values of $\mathcal{F}$ and $\mathcal{P}$, at which $\widetilde{\mathcal{L}}_{\sigma}(\mathcal{F}, \mathcal{P}, \mathcal{Z}, \boldsymbol{\lambda})$ is not continuous or not differentiable. At such non-smooth points, $\widetilde{\mathcal{L}}_{\sigma}(\mathcal{F}, \mathcal{P}, \mathcal{Z}, \boldsymbol{\lambda})$ can attain its local minimum value. Thus, in the following, we mainly analyze the local optimality of the unconstrained $\widetilde{\mathcal{L}}_{\sigma}(\mathcal{F}, \mathcal{P}, \mathcal{Z}, \boldsymbol{\lambda})$ at the smooth points.

Theorem 1. Suppose that $V(\mathcal{F}, \mathcal{P})$ is continuously twice differentiable at a feasible $\mathcal{F}^*$ and a feasible $\mathcal{P}^*$, and there also exist some feasible $\mathcal{Z}^*$ and $\boldsymbol{\lambda}^*$ such that $\mathcal{F}^*$ and $\mathcal{P}^*$ satisfy the second-order sufficient optimality conditions of (32). There must exist a positive $\sigma^* > 0$ such that $\mathcal{F}^*$ and $\mathcal{P}^*$ are a strict local minima of the following unconstrained optimization

$$
\min_{\mathcal{F}, \mathcal{P}} : \ \widetilde{\mathcal{L}}_{\sigma}(\mathcal{F}, \mathcal{P}, \mathcal{Z}^*, \boldsymbol{\lambda}^*)
\tag{38}
$$

for any $\sigma \geq \sigma^*$. In addition, if there exist a feasible $\bar{\mathcal{F}}$ and a feasible $\bar{\mathcal{P}}$, i.e., meeting $\phi_{l,i}(k) = 0$ for all $l = 1, \ldots, 4$, $i \in \mathcal{N}$, and $k \in \mathcal{K}$, which are a local minima of

$$
\min_{\mathcal{F}, \mathcal{P}} : \ \widetilde{\mathcal{L}}_{\bar{\sigma}}(\mathcal{F}, \mathcal{P}, \bar{\mathcal{Z}}, \bar{\boldsymbol{\lambda}})
\tag{39}
$$

for some $\bar{\mathcal{Z}}$, $\bar{\sigma} > 0$ and $\bar{\boldsymbol{\lambda}}$, $\bar{\mathcal{F}}$ and $\bar{\mathcal{P}}$ must also be a local minima of (32).

Theorem 2. There must exist a positive $\sigma^* > 0$ such that for any $\sigma \geq \sigma^*$, a local minimum point obtained by solving the following unconstrained problem

$$
\min_{\mathcal{F}, \mathcal{P}, \boldsymbol{\lambda}} : \ \mathcal{L}_{\sigma}(\mathcal{F}, \mathcal{P}, \boldsymbol{\lambda})
\tag{40}
$$

is also a local minimum point of (32).

The proofs of Theorems 1 and 2 can be found in Appendices D and E in the supplementary material, respectively.

Based on these two theorems, it is observed that solving the constrained (32) can be achieved by solving the unconstrained (40) that does not require an infinite positive penalty factor. Instead, in (40), the penalty factor σ is only a sufficiently large but finite positive number. Such a property is quite important since it allows us to practically design as well as implement an iterative algorithm to approach the locally optimal solution of (32). Let $\mathcal{F}[\tau]$, $\mathcal{P}[\tau]$ and $\boldsymbol{\lambda}[\tau]$ be the feasible points and Lagrangian multipliers obtained at the τ-th iteration, which satisfy the conditions in Theorem 1. From (S.10), we can get

$$
\nabla_{\mathcal{S}} V(\mathcal{F}[\tau], \mathcal{P}[\tau]) - \Phi(\mathcal{S})(\boldsymbol{\lambda}[\tau] - \sigma \boldsymbol{\phi}(\mathcal{F}[\tau], \mathcal{P}[\tau])) = \boldsymbol{0},
\tag{41}
$$

where $\boldsymbol{\phi}(\mathcal{F}[\tau], \mathcal{P}[\tau])$ denotes the value of ϕ evaluated at the specific points $\mathcal{F}[\tau]$ and $\mathcal{P}[\tau]$ at iteration τ.

On the other hand, from Theorem 1, $\bar{\mathcal{F}}$, $\bar{\mathcal{P}}$ and $\bar{\boldsymbol{\lambda}}$ are the local minimizer of (32), such that we also derive the gradient condition of its Lagrangian function (36), i.e.,

$$
\nabla_{\mathcal{S}} V(\bar{\mathcal{F}}, \bar{\mathcal{P}}) - \Phi(\mathcal{S})\bar{\boldsymbol{\lambda}} = \boldsymbol{0}.
\tag{42}
$$

By comparing (42) and (41), we can see that the convergence condition of iterations on the Lagrangian multipliers $\boldsymbol{\lambda}[\tau]$ is enforcing $\boldsymbol{\phi}(\mathcal{F}[\tau], \mathcal{P}[\tau]) \to \boldsymbol{0}$ as $\tau \to \infty$. Therefore, we derive the iterative formula for the Lagrangian multipliers as follows

$$
\boldsymbol{\lambda}[\tau + 1] = \boldsymbol{\lambda}[\tau] - \sigma \boldsymbol{\phi}(\mathcal{F}[\tau], \mathcal{P}[\tau]), \ \tau \in \mathbb{Z}_{>0}.
\tag{43}
$$

Recall the definition of $\phi_{l,i}(k)$, i.e., $\phi_{l,i}(k) = \mu_{l,i}(k) - z_{l,i}^2(k)$, and the derivation of the auxiliary variable $z_{l,i}^2(k)$ in (S.4). Substituting the expression of $z_{l,i}^2(k)$ into $\phi_{l,i}(k)$, we can further re-arrange (43) as

$$
\lambda_{l,i,\tau+1}(k) = \begin{cases} \lambda_{l,i,\tau}(k) - \sigma \mu_{l,i,\tau}(k), & \lambda_{l,i,\tau}(k) \geq \sigma \mu_{l,i,\tau}(k); \\ 0, & \text{otherwise.} \end{cases}
\tag{44}
$$

for all $l = 1, \ldots, 4$, $i \in \mathcal{N}$, $k \in \mathcal{K}$, and $\tau \in \mathbb{Z}_{>0}$, where we use $\lambda_{l,i,\tau}(k)$ and $\mu_{l,i,\tau}(k)$ to denote $\lambda_{l,i}(k)$ and $\mu_{l,i}(k)$ evaluated at iteration τ, respectively.

To measure the convergence performance, we introduce a stop criterion for iterations as ε_τ based on (44)

$$
\varepsilon_\tau = \left(\sum_{k \in \mathcal{K}} \sum_{i \in \mathcal{N}} \sum_{l=1}^{4} \xi_{l,i,\tau}^2(k) \right)^{\frac{1}{2}},
\tag{45}
$$

where $\xi_{l,i,\tau}(k)$ is defined as

$$
\xi_{l,i,\tau}(k) = \begin{cases} \mu_{l,i,\tau}(k), & \lambda_{l,i,\tau}(k) \geq \sigma \mu_{l,i,\tau}(k); \\ \frac{\lambda_{l,i,\tau}(k)}{\sigma}, & \text{otherwise.} \end{cases}
\tag{46}
$$

Thus, given a tolerance $\epsilon > 0$ where ϵ is a sufficiently small number, the iterations $\{\mathcal{F}[\tau], \mathcal{P}[\tau], \boldsymbol{\lambda}[\tau], \tau \in \mathbb{Z}_{>0}\}$ is considered to converge when $\varepsilon_\tau \leq \epsilon$ is met at a certain τ.

Now, based on the theorems presented above, we propose an iterative method as shown in Figure 2, which combines by exploiting a derivative-free optimization technique to solve the unconstrained optimization to approach the optimal solution of the original problem (32). In addition, we also use the stop criterion based on ε_τ to adapt the
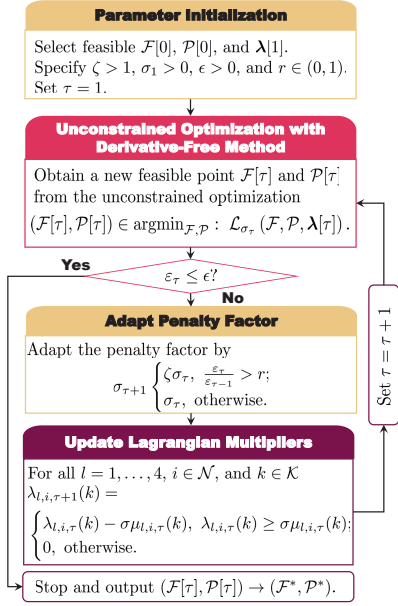
Fig. 2. The high-level LTE-V2V communication optimization approach.

updating of the penalty factor. It is remarked that there currently exist many well-known derivative-free optimization methods, such as generalized pattern search (GPS), simulated annealing (SA), particle swarm optimization (PSO). Our model transformation enables these derivative-free optimization methods to solve the subproblem, which do not need any information on the gradient of the non-smooth objective function $V(\mathcal{F}, \mathcal{P})$.

3.3 Joint Optimization Method of Vehicular Communication and Macroscopic Traffic Control

Combining the low-level and high-level models above, we develop a joint optimization framework of vehicular communication and macroscopic traffic control as in Figure 3. According to much literature from transportation science [10], [13], [21], [57], [59], [60], the multi-region MFDs can be easily estimated by using real-time measurements from road traffic sensors such as loop detectors, vehicles' GPS trajectories, and road-side video monitors. Many existing advanced estimation techniques, including the nonlinear horizon estimation approach [60], can also be applied to obtain origin-destination (OD) demands and traffic accumulation in our urban cities. [59] also shows that we can use an unscented Kalman filter (UKF) to enhance the accuracy in estimating average trip length and traffic accumulations, providing the basis for the practical realization of MFD-based perimeter flow control. In the implementation framework, a central cloud server is considered to collect real-time traffic data of the multiple urban regions via traffic sensors and then solve the MFD-based MPC model (30) to obtain a sequence of perimeter control inputs $\mathcal{U}^*$ over the prediction horizon. The low-level MPC model also feedbacks the predicted traffic flow dynamics as well as the perimeter control inputs to the high-level vehicular communication optimization model (40), driving the high-level model to get the optimal frequency and power solutions $(\mathcal{F}^*, \mathcal{P}^*)$. The joint optimization solution sequences $\{\mathcal{F}^*, \mathcal{P}^*, \mathcal{U}^*\}$ are distributed

to the road-side resource management infrastructures (e.g., eNodeBs) of the LTE-V2V networks and the perimeter controllers, respectively. For real-time implementation, only the first communication and control actions in the solution sequences, $\boldsymbol{f}^*(0) \in \mathcal{F}^*$, $\boldsymbol{p}^*(0) \in \mathcal{U}^*$, $\boldsymbol{u}^*(0) \in \mathcal{U}^*$, are applied by the execution entities (i.e., the LTE eNodeBs and perimeter controllers), and the joint optimization procedure is carried out again by moving the prediction horizon.[4]

For the joint optimization framework, we can have the following property to characterize the obtained joint solution $\{\mathcal{F}^*, \mathcal{P}^*, \mathcal{U}^*\}$. The corresponding proof is provided in Appendix F in the supplementary material.

Theorem 3. Suppose that $\mathcal{U}^*$ is obtained from the receding horizon optimization (30) satisfying $C(\mathcal{U}^*) < C(\mathcal{U})$, and $\{\mathcal{F}^*, \mathcal{P}^*\}$ are obtained from the unconstrained optimization (40) with the specified perimeter control $\mathcal{U}^*$. $\{\mathcal{F}^*, \mathcal{P}^*, \mathcal{U}^*\}$ constitute a Pareto-optimal feasible solution for the original system model (27).

Interestingly, the joint solution $\{\mathcal{F}^*, \mathcal{P}^*, \mathcal{U}^*\}$ obtained by our proposed framework is also a Nash equilibrium by definition, when we treat the bi-level optimization problem as a special form of Stackelberg game. That is, two interactive agents, a high-level leader and a low-level follower, implement the communication optimization and the traffic control of the multiple regions, respectively. A game-theoretical interpretation is that the leader optimizes its own actions $\{\mathcal{F}, \mathcal{P}\}$, given that the follower optimizes its own actions $\{\mathcal{U}\}$. With the joint actions $\{\mathcal{F}^*, \mathcal{P}^*, \mathcal{U}^*\}$, both the agents reach a Nash equilibrium since they cannot improve their own individual objective unilaterally without deteriorating the other's individual objective.

4 PERFORMANCE EVALUATION

This section provides simulation results on the performance comparison between our proposed method and others. The online supplementary material presents expanded results with different scenario configurations in Appendix H.

4.1 Simulation Settings

For simulation demonstration, we consider a three-region urban traffic network, $\mathcal{N} = \{1, 2, 3\}$, where each region is adjacent to the others and all the regions have different MFDs. We refer to the shape of the empirical MFD observed in Yokohama as reported in [23], which can be well characterized by the following three-order polynomial [21]

$$g_{\text{Yok}}(x(k)) = \frac{1.4877 \times 10^{-7} x^3(k) - 2.9815 \times 10^{-3} x^2(k) + 15.0912 x(k)}{3600}$$

(47)

---

4. In macroscopic traffic control, the central cloud is deployed in a city's traffic management center (TMC). This center is the hub of the city's traffic control system connected to signal controllers at each intersection of the road network [67]. The traffic control signal is transmitted via wire connections (e.g., fiber-optic communication) from the center to those traffic controllers. Thus, in such a centralized architecture, the end-to-end latency between the control activation in different regions is minor. Considering large-scale deployment and hierarchical control architectures, the impact of control signal transmission delays, even in the order of several hundred milliseconds, can be reasonably neglected since the traffic signals are generally operated on a cycle duration of several tens of seconds [10]–[13].
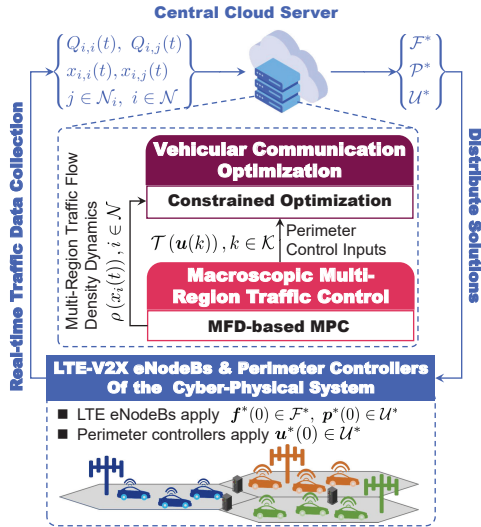
Fig. 3. The implementation framework of our joint optimization method.

TABLE 2
Parameter Settings for MPC-based Perimeter Flow Control

Parameter	Value	Parameter	Value
$\boldsymbol{x}(0)$	$[1,3,5]^{\mathrm{T}} \times 10^3$ (veh)	ΔT	$50\,\mathrm{s}$
$[u_{i,j}^-, u_{i,j}^+]$	$[0,1]$	K_p	30
$[x_i^-, x_i^+]$	$[0,10^4]$ (veh)	$[x_{i,j}^-, x_{i,j}^+]$	$[0,10^4]$ (veh)

TABLE 3
Simulation Settings on $m_{\mathrm{RB}}^{\mathrm{beacon}}(L_{\mathrm{size}}, I_{\mathrm{MCS}})$ with the fixed beacon size $L_{\mathrm{size}} = 200\,\mathrm{bytes}$ over $10\,\mathrm{MHz}$ channel

I_{MCS}	Modulation	$m_{\mathrm{RB}}^{\mathrm{beacon}}$	$\gamma_{\min}$
1	QPSK	72	$-0.21\,\mathrm{dB}$
2	16-QAM	16	$12.85\,\mathrm{dB}$

TABLE 4
Parameter Settings for LTE-V2V Communications

Parameter	Value	Parameter	Value
g_0	$3\,\mathrm{dB}$	L_0	$47.86\,\mathrm{dB}$
α	2.75	σ_i^2	$-95\,\mathrm{dBm}$
L_{size}	$200\,\mathrm{bytes}$	R_0	$200\,\mathrm{m}$

that attains the maximum level $g_{\mathrm{Yok}}(x_{\mathrm{Yok,cr}}) = 6.3\,\mathrm{veh/s}$ at the critical accumulation $x_{\mathrm{Yok,cr}} = 3400\,\mathrm{veh}$. The accumulation at the jammed traffic density is about $x_{\mathrm{Yok}}^+ = 10000\,\mathrm{veh}$. Thus, to simulate different MFD shapes of the urban regions, we introduce a scaling factor $\xi_i > 0$ and set their MFDs to $g_i(x_i(k)) = \xi_i g_{\mathrm{Yok}}(x_i(k))$ for each $i \in \mathcal{N}$. Similar to the simulation settings in [57], we specify $\xi_1 = 1.2$ for the region $i = 1$, $\xi_2 = 1.0$ for $i = 2$ and $\xi_3 = 0.8$ for $i = 3$. Figure 4 shows the MFDs of the multiple urban regions in our simulations. The time-varying traffic flow demands over the time horizon $[0, 12000]\,(\mathrm{s})$ are shown in Figure 5, which simulate the non-peak-hour and peak-hour situations. Other parameter settings used in predictive perimeter control are summarized in Table 2 based on the current literature.[5]

We take into consideration two types of the MCSs, i.e., a Quadrature Phase Shift Keying (QPSK)-based MCS and a Quadrature Amplitude Modulation using 16 different phase-amplitude combinations (16-QAM). Following [8],

---

5. The duration of each time step in implementing the predictive perimeter control is usually configured according to the time resolution of macroscopic traffic flow data collected by road traffic sensors and the control cycle of signalized intersections. According to much current literature [10], [11], [13], [21], [60], this time duration is in the order of several tens of seconds in large-scale urban road networks. For example, Reference [21] configures their controller's time step to a cycle duration of typical signalized intersections, 60 s. [10] sets the duration of each control step to about 50 s, while [13] uses a longer control interval, i.e., 180 s. Thus, since the predictive perimeter controller drives the EE optimization model, the communication optimization is performed per perimeter control cycle.

Numerous studies on perimeter traffic flow control in transportation science employ simulation-based approaches to validate their models and control schemes, particularly considering large-scale urban macroscopic traffic control scenarios. For example, [13] partitions the road traffic network of Downtown San Francisco into two regions for their simulations. References [10], [19], [21], [54], [63] also consider two-region case studies. In [12], the researchers partition their test site into three regions. Following these existing studies, we consider a three-region case study for performance demonstration. In our paper, the parameters for macroscopic traffic flow simulations are referred to in the existing literature, such as [21], [23], [57]. The communication parameters are configured according to Release 14 of LTE-V2V communication standard introduced by 3GPP. The communication settings are also adopted in many other studies, such as [8], [35]. Other simulation scenarios do not alter our proposed methodology.

the number of the RB allocated for broadcasting a beacon, $m_{\mathrm{RB}}^{\mathrm{beacon}}(L_{\mathrm{size}}, I_{\mathrm{MCS}})$, and the minimal SINR requirement, $\gamma_{\min}$, under these two different MCSs are given in Table 3. Other parameter settings for LTE-V2V communications are also referred to in the existing literature and the 3GPP standard specification [8], [46], [68], as given in Table 4.

4.2 Performance Verification

4.2.1 Model predictive perimeter control

We use the aforementioned case study to compare the effect of the model predictive perimeter control to a baseline in which the perimeter traffic flows are not restricted. Figures 6 to 8 show the model predictive perimeter control inputs of each urban region and the evolution of the transfer traffic flows from each region with and without the model predictive perimeter control over the simulation horizon. Figure 6 shows the evolution of the multi-region transfer traffic flows without the perimeter control. It is witnessed for this non-control case that the urban region $i = 3$ experiences traffic congestion or even gridlock after about $3000\,\mathrm{s}$ due to its increasing transfer flows received from the other two regions. By comparison, Figures 7 and 8 shows the effect of the MPC-based perimeter control method. From Figure 7, it is seen that most of the perimeter transfer flows from the three urban regions are promoted with the 100% control except those from the regions $i = 1, 2$ to the region $i = 3$. In particular, the perimeter controls on the transfer flows from the regions 1 and 2 to the region 3, $u_{1,3}(t)$ and $u_{2,3}(t)$, decrease at about $1350\,\mathrm{s}$ and $800\,\mathrm{s}$, respectively. This is because the total exogenous traffic demands from the regions $i = 1, 2$ to the region $i = 3$ significantly grow as shown in Figure 5. The transfer flows to $i = 3$ are restricted by the perimeter controllers of the regions $i = 1, 2$ in order to avoid the
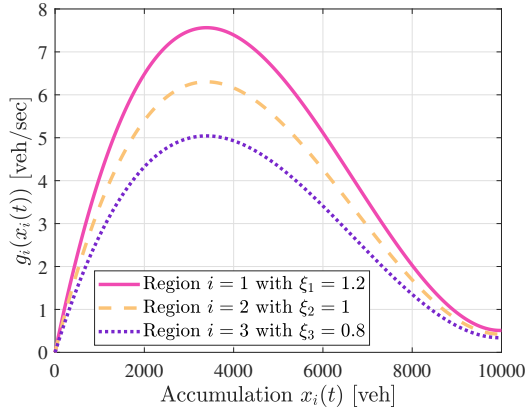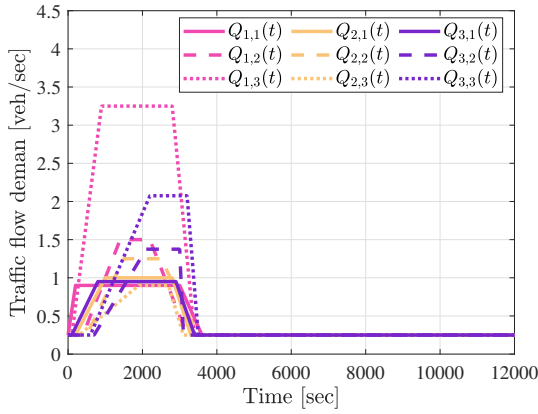
Fig. 4. The MFDs of a three-region urban area.

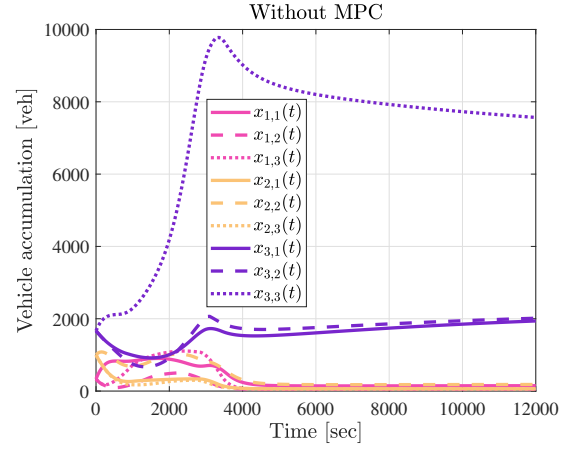Fig. 5. The time-varying traffic demands of the three urban regions.

Fig. 6. The dynamics of the transfer flows from each urban region without the MPC-based perimeter control.
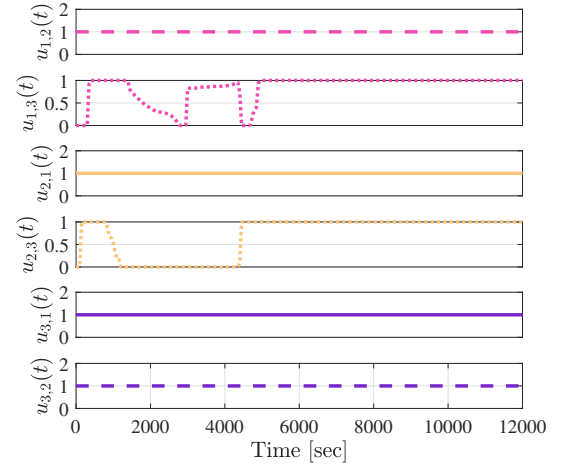

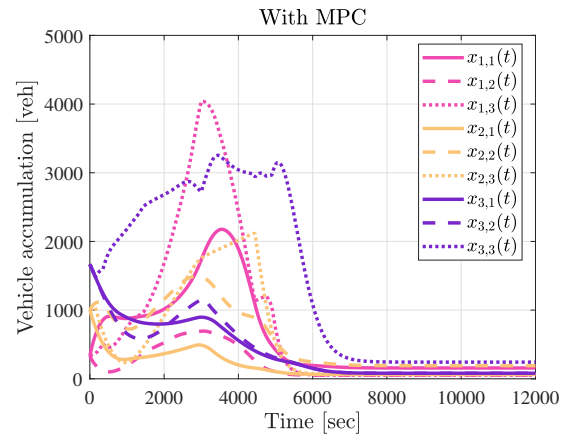
Fig. 7. The perimeter control inputs of the urban regions.

Fig. 8. The dynamics of the transfer flows from each urban region with the MPC-based perimeter control.

traffic congestion in their destination region. From Figure 8, it can be observed that the transfer flows of all the urban regions can be stabilized and maintained below the level of $1000 \, \text{veh}$ after about $6000 \, \text{s}$ under the MPC-based perimeter control. In addition, the vehicle accumulation of each region does not exceed the jam point, i.e., $x_i^+ = 10000 \, \text{veh}$, and the model predictive perimeter control method is shown to clear the traffic network in Figure 8. It is apparent that utilizing the model predictive perimeter control based on the multi-region MFDs can reduce vehicles' trip delays and thus improve the system performance in terms of road traffic efficiency.

4.2.2 Vehicular communication optimization

To verify the high-level LTE-V2V communication optimization method, we use the snapshot of the multi-region traffic flow dynamics at the beginning time instant (i.e., at $t = 0 \, \text{s}$) as the input information of the proposed optimization method. The feasible region of the transmission power is set to $[-30, 20] \, (\text{dB})$ and that of the broadcast beacon frequency is $[1, 100] \, (\text{Hz})$. Figures 9 and 10 show the EE distribution snapshot of each region's LTE-V2V network as well as the EE optimization convergence behaviors under both QPSK and 16-QAM MCSs. From the heatmaps of Figure 9, we can see that the EE peak of the region $i = 1$ is higher than those of the regions $i = 2, 3$. The underlying reason

is that the vehicle accumulation of $i = 1$ at the snapshot is lower than the other two urban regions as shown in Figure 8, and more RBs of the LTE network can be allocated to each vehicle in $i = 1$. The contours in the heatmaps also
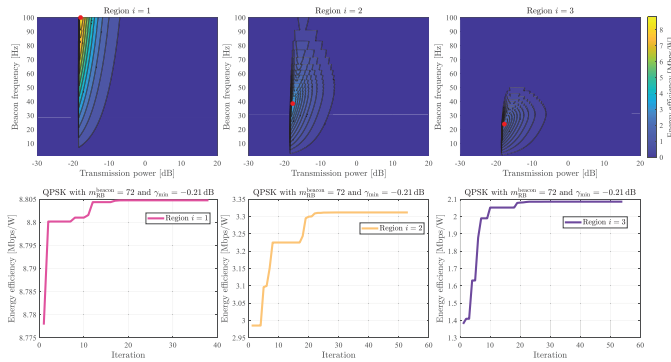
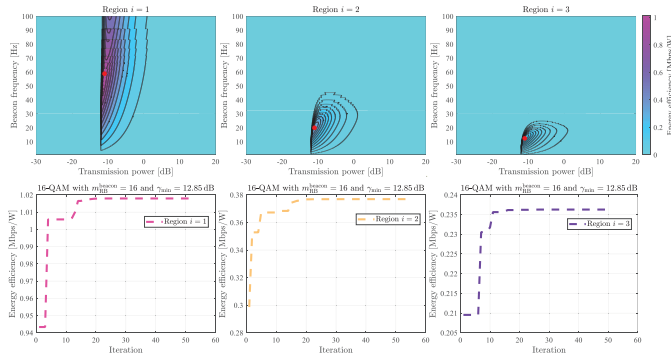Fig. 9. The convergence of the vehicular communication optimization with QPSK MCS.

Fig. 10. The convergence of the vehicular communication optimization with 16-QAM MCS.

indicate that the EE distribution per urban region is a non-smooth and nonlinear function with respect to the power and frequency decision variables. Figure 9 also shows that a higher beacon frequency of LTE-V2V communications can be supported by more allocated RBs and thus improve the cooperative awareness among LTE-V2V vehicles. Besides, it is observed that our proposed optimization method can stably converge to the global optimal EE point of all the urban regions only after several tens of iterations. Figure 10 also shows the similar results. By comparison, the EE peaks of the multi-region LTE-V2V networks under the 16-QAM MCS are lower than those under the QPSK. The main reason is that the QPSK MCS can have more RBs for allocating a beacon (as reported in Table 3) and the number of vehicles to be effectively supported in the LTE resource reuse range increases. Hence, the QPSK MCS allows more LTE-V2V vehicles per urban region and improves the network EE under the same vehicle density. Together, the results from both Figures 9 and 10 verify the highly-efficient global convergence of the proposed method for the high-level LTE-V2V communication optimization of the multiple regions even with a constrained non-smooth EE objective function.

4.3 Performance Comparison

To demonstrate the performance of our proposed method, the VCOMTC, as detailed in Figure 3, we use a case study that follows the simulation settings in Subsection 4.1 to compare our method to two other baselines and one another strong method. One baseline method follows the vehicu-

lar communication standard to adopt a constant power of $p_i(t) = 23\,\mathrm{dBm}$ while a conservative beacon frequency of $f_i(t) = 10\,\mathrm{Hz}$ for all i and t for the high-level LTE-V2V communications, and also integrates such Conservative Communication Policy (CCP) with the multi-region model predictive perimeter control. The other baseline also uses the same transmission power but a more aggressive beacon frequency, $100\,\mathrm{Hz}$, and also combines such Aggressive Communication Policy (ACP) with the MPC-based perimeter control. For a better understanding of the joint optimization impact, we further implement another strong method for vehicular communication optimization, denoted by VCO, that uses the advanced Lagrangian constrained optimization at the high level for the multi-region LTE-V2V communications but without integrating the multi-region perimeter control at the low level.[6]

Figure 11 compares the evolution of the EE metric per urban region over the simulation horizon under these comparative methods. As can be seen, the two baselines, the CCP and the ACP methods, perform worse than the other two implementing the high-level vehicular communication optimization, since they use constant power and frequency policies and cannot optimize the LTE-V2V resource allocation dynamically, even though integrating the model predictive perimeter control at the low level. Our proposed method, the VCOMTC, optimizes the multi-region EE performance dynamically and is able to adapt to the time-varying spatial distribution of vehicles by using the MPC-based multi-region perimeter control at the low level. When the transfer traffic flows are stabilized and the vehicle accumulation per region under the low-level perimeter control converges to the lowest level after about $8000\,\mathrm{s}$ as illustrated in Figure 8, the EE metric of the joint optimization method reaches at the maximal level. From Figure 11, it is seen that, when the vehicle densities of these urban regions grow due to their increasing traffic demands, e.g., within about $[2000, 4000]\,(\mathrm{s})$ as in Figure 5, the EE metrics of the regions decrease, since the LTE-V2V resources are limited. Figure 11 also shows that the EE metrics of the regions under the comparative methods using the QPSK are higher than those using the 16-QAM on average. This is due to the fact that the QPSK MCS can allocate more RBs for broadcasting beacons and improve the communication capacity compared to the 16-QAM. By comparison, the VCO method can achieve higher EE than our method for the specific regions $i = 1, 2$ during the first $7000\,\mathrm{s}$. The main reason is that the VCO without the low-level model predictive perimeter control does not restrict the perimeter transfer flows and thus drives the vehicle accumulations of the regions $i = 1, 2$ to a lower level during the beginning time horizon, in particular within $[1000, 7000]\,(\mathrm{s})$ as shown in Figure 6. However, even though our joint optimization method experiences a worse-EE stage since the controlled regions $i = 1, 2$ preserve slightly more vehicle accumulations within $[1000, 7000]\,(\mathrm{s})$, the proposed method

6. The baseline methods are implemented based on the LTE-V2V communication standard, which are also widely employed in the literature, such as [1], [3], [8], for performance comparison. Besides, the advanced method for performance comparison follows the state-of-the-art resource optimization approach, the Lagrangian constrained optimization, to optimize power and radio resources, which has also been widely investigated in the related works [26], [27], [40].

using the model predictive perimeter control stabilizes the vehicle accumulations of $i = 1, 2$ to the low level and thus can achieve the high EE performance similar to that of the VCO method after $7000\,$s. More importantly, for the region $i = 3$, the proposed joint optimization method can achieves much higher EE performance than the VCO, in particular after about $1000\,$s. When using our VCOMTC, the high-level communication optimization is driven by the low-level macroscopic traffic control and the system dynamically adapts the global vehicle accumulations to avoid congested traffic or gridlock in each region. Hence, as shown in Figures 5 and 8, the vehicle accumulation of the region $i = 3$ is stabilized to a much lower level by using the MPC-based perimeter control compared to that in Figure 6, even though this region experiences higher exogenous traffic demands. The VCO without the perimeter control cannot suppress the overshoot in the vehicular accumulation of $i = 3$ and experiences heavy traffic jam, which, in turn, leads to a remarkable decrease in the region EE performance. In particular, since the limited LTE resources are not sufficient to support the massive jammed traffic in the region $i = 3$, the VCO method even performs worse than the baseline method, i.e., the ACP. It is obvious that integrating the low-level model predictive perimeter control with the high-level vehicular communication optimization better benefits the system from the perspectives of improving the region traffic efficiency and EE performance.

To provide better insight into the strength of the proposed method, we further report two system-level key performance indicators (KPIs), the accumulated energy efficiency over the whole simulation time and the fairness index in resource utilization[7]. Figure 12 shows that both our VCOMTC and the VCO methods produce much higher EE than the other two baselines. Specifically, the accumulated EE metric achieved by our VCOMTC is about 12.24% and 9.57% higher than that by the VCO under the QPSK and the 16-QAM, respectively. In Figure 13, we compare the fairness indexes of our method and the VCO in terms of resource utilization over time. It is observed that the fairness index of the VCOMTC is always higher than that of the VCO and can stably converge to the maximal level, i.e., the 100%-fairness level, after about $7000\,$s under either the QPSK or the 16-QAM cases. By contrast, the VCO reduces the fairness index and can maintain the fairness level of only 72.31% and 69.75% during the last $5000\,$s under the QPSK and the 16-QAM, respectively. The main reason is that using the low-level MPC-based perimeter control is better able to balance the traffic flow distributions over the multiple urban regions so as to minimize the system-wide traffic delays. Different from the VCO without the perimeter control, the VCOMTC method avoids traffic congestion and accumulation overshoot in each region and finally arrives at the multi-region consensus in their temporal-spatial traffic distribu-

7. Since the vehicle density and traffic flow of the multiple regions differ from each other, the EE performance of these regions' LTE-V2V networks is also different. Unfair resource utilization will result in uneven EE performance distribution over these regions. Thus, we resort to Jain's fairness index, a well-known metric used for measuring the fairness of resource allocation among multiple systems, to demonstrate the ability of different methods to guarantee even performance distribution. The formulation of the fairness index is detailed in Appendix G in the supplementary material.
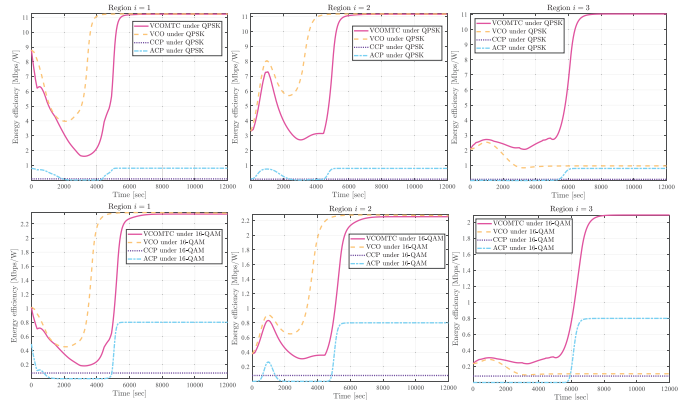

Fig. 11. The evolution of the multi-region EE metrics under comparative methods.
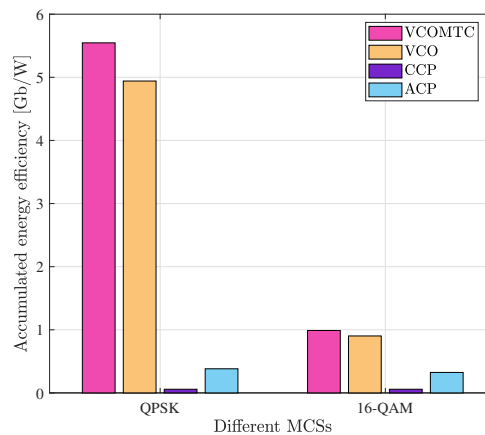

Fig. 12. The system-level accumulated EE under comparative methods.

tions. The high-level LTE-V2V communication optimization of the multiple regions is dynamically driven by the multi-region traffic dynamics under the low-level model predictive perimeter control. Therefore, the VCOMTC method guarantees much better fairness in the LTE-V2V communication resource utilization for multi-region EE optimization. These results together verify the remarkable benefit brought by joining the macroscopic traffic control with the vehicular communication optimization in the hierarchical framework.

5 CONCLUSION AND FUTURE WORK

In this paper, we focus on cooperative awareness of connected vehicles based on LTE-V2V communication networks and propose an MPC-based hierarchical framework that joins the perimeter traffic flow control using the MFDs of multiple urban regions into the holistic EE optimization of the multi-region LTE-V2V communication networks. Our method integrates the multi-region traffic flow dynamics under control to drive vehicular EE communication optimization. The proposed joint optimization design enables multi-region LTE-V2V communications to adapt to the temporal-spatial macroscopic traffic evolution, provides insight into the coupling between the communication networks and traffic networks, and improves existing solutions. Using simulation experiments, we show that our joint
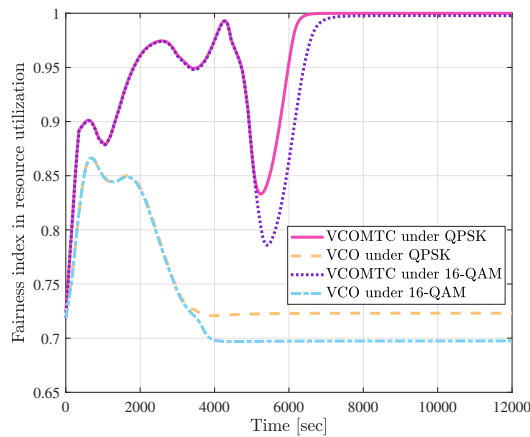
Fig. 13. The evolution of Jain's fairness index in resource utilization under comparative methods.

optimization method, compared to existing approaches, provides balanced temporal-spatial traffic flows, improved global EE communication performance, and better global fairness in network resource utilization. However, challenges remain for our proposed approach to systematically optimizing connected vehicles, such as the need for distributed or decentralized computation and synchronization in controlling and optimizing large-scale networks. As a potential direction in future work, event-triggered MPC control approaches can also be developed for perimeter flow control and thus combined with the EE optimization of vehicular networks.

ACKNOWLEDGMENTS

REFERENCES

[1] S. Chen, J. Hu, Y. Shi, and L. Zhao, "Lte-v: A td-lte-based v2x solution for future vehicular network," *IEEE Internet of Things Journal*, vol. 3, no. 6, pp. 997–1005, Dec 2016.

[2] A. C. Barranco, J. A. Y. Gálvez, J. A. Armijo, M. C. Aguayo-Torres, J. C. R. Sicilia, and G. Gómez, "Overview of lte for vehicular communications," *Wireless Personal Communications*, vol. 113, no. 3, pp. 1471–1494, April 2020.

[3] R. Molina-Masegosa and J. Gozalvez, "Lte-v for sidelink 5g v2x vehicular communications: A new 5g technology for short-range vehicle-to-everything communications," *IEEE Vehicular Technology Magazine*, vol. 12, no. 4, pp. 30–39, Dec 2017.

[4] S. Gyawali, S. Xu, Y. Qian, and R. Q. Hu, "Challenges and solutions for cellular based v2x communications," *IEEE Communications Surveys Tutorials*, vol. 23, no. 1, pp. 222–255, Firstquarter 2021.

[5] D. Niyato, E. Hossain, and P. Wang, "Optimal channel access management with qos support for cognitive vehicular networks," *IEEE Transactions on Mobile Computing*, vol. 10, no. 4, pp. 573–591, April 2011.

[6] J. Zhou, D. Tian, Y. Wang, Z. Sheng, X. Duan, and V. C. Leung, "Reliability-optimal cooperative communication and computing in connected vehicle systems," *IEEE Transactions on Mobile Computing*, vol. 19, no. 5, pp. 1216–1232, May 2020.

[7] H. Mosavat-Jahromi, Y. Li, Y. Ni, and L. Cai, "Distributed and adaptive reservation mac protocol for beaconing in vehicular networks," *IEEE Transactions on Mobile Computing*, vol. 20, no. 10, pp. 2936–2948, Oct 2021.

[8] A. Bazzi, B. M. Masini, A. Zanella, and I. Thibault, "On the performance of ieee 802.11p and lte-v2v for the cooperative awareness of connected vehicles," *IEEE Transactions on Vehicular Technology*, vol. 66, no. 11, pp. 10 419–10 432, Nov 2017.

[9] M. Gonzalez-Martín, M. Sepulcre, R. Molina-Masegosa, and J. Gozalvez, "Analytical models of the performance of c-v2x mode 4 vehicular communications," *IEEE Transactions on Vehicular Technology*, vol. 68, no. 2, pp. 1155–1166, Feb 2019.

[10] M. Ramezani, J. Haddad, and N. Geroliminis, "Dynamics of heterogeneity in urban networks: aggregated traffic modeling and hierarchical control," *Transportation Research Part B: Methodological*, vol. 74, pp. 1–19, 2015. [Online]. Available: https://www.sciencedirect.com/science/article/pii/S0191261515000028

[11] M. Yildirimoglu, I. I. Sirmatel, and N. Geroliminis, "Hierarchical control of heterogeneous large-scale urban road networks via path assignment and regional route guidance," *Transportation Research Part B: Methodological*, vol. 118, pp. 106–123, 2018. [Online]. Available: https://www.sciencedirect.com/science/article/pii/S0191261518301152

[12] K. Aboudolas and N. Geroliminis, "Perimeter and boundary flow control in multi-reservoir heterogeneous networks," *Transportation Research Part B: Methodological*, vol. 55, pp. 265–281, 2013. [Online]. Available: https://www.sciencedirect.com/science/article/pii/S0191261513001185

[13] K. Ampountolas, N. Zheng, and N. Geroliminis, "Macroscopic modelling and robust control of bi-modal multi-region urban road networks," *Transportation Research Part B: Methodological*, vol. 104, pp. 616–637, 2017. [Online]. Available: https://www.sciencedirect.com/science/article/pii/S0191261515300370

[14] Z. Hou and T. Lei, "Constrained model free adaptive predictive perimeter control and route guidance for multi-region urban traffic systems," *IEEE Transactions on Intelligent Transportation Systems*, pp. 1–13, 2020.

[15] H. Mustakim, "5g vehicular network for smart vehicles in smart city: A review," *Journal of Computer, Electronic, and Telecommunication*, vol. 1, pp. 1–6, 07 2020.

[16] N. Aljeri and A. Boukerche, "Mobility management in 5g-enabled vehicular networks: Models, protocols, and classification," *ACM Comput. Surv.*, vol. 53, no. 5, sep 2020. [Online]. Available: https://doi.org/10.1145/3403953

[17] X. Cheng, R. Zhang, and L. Yang, *Wireless-Vehicle Combination: Effective MAC Designs in VCN*. Cham: Springer International Publishing, 2019, pp. 87–134. [Online]. Available: https://doi.org/10.1007/978-3-030-02176-4_4

[18] A. Bazzi, A. O. Berthet, C. Campolo, B. M. Masini, A. Molinaro, and A. Zanella, "On the design of sidelink for cellular v2x: A literature review and outlook for future," *IEEE Access*, vol. 9, pp. 97 953–97 980, 2021.

[19] J. Haddad, "Optimal perimeter control synthesis for two urban regions with aggregate boundary queue dynamics," *Transportation Research Part B: Methodological*, vol. 96, pp. 1–25, 2017. [Online]. Available: https://www.sciencedirect.com/science/article/pii/S0191261516308025

[20] R. Zhong, C. Chen, Y. Huang, A. Sumalee, W. Lam, and D. Xu, "Robust perimeter control for two urban regions with macroscopic fundamental diagrams: A control-lyapunov function approach," *Transportation Research Part B: Methodological*, vol. 117, pp. 687–707, 2018, tRB:ISTTT-22. [Online]. Available: https://www.sciencedirect.com/science/article/pii/S0191261517307671

[21] N. Geroliminis, J. Haddad, and M. Ramezani, "Optimal perimeter control for two urban regions with macroscopic fundamental diagrams: A model predictive approach," *IEEE Transactions on Intelligent Transportation Systems*, vol. 14, no. 1, pp. 348–359, March 2013.

[22] J. Godfrey, "The mechanism of a road network," *Traffic Engineering and Control*, vol. 11, no. 7, pp. 323–327, Nov 1969.

[23] N. Geroliminis and C. F. Daganzo, "Existence of urban-scale macroscopic fundamental diagrams: Some experimental findings," *Transportation Research Part B: Methodological*, vol. 42, no. 9, pp. 759–770, 2008. [Online]. Available: https://www.sciencedirect.com/science/article/pii/S0191261508000180

[24] N. Geroliminis, "Dynamics of peak hour and effect of parking for congested cities," *Transportation Research Board Annual Meeting 2009*, no. 09-1685, 2009. [Online]. Available: http://infoscience.epfl.ch/record/141817

[25] N. Geroliminis and J. Sun, "Properties of a well-defined macroscopic fundamental diagram for urban traffic,"

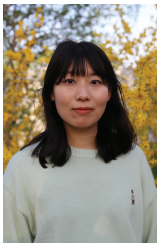*Transportation Research Part B: Methodological*, vol. 45, no. 3, pp. 605–617, 2011. [Online]. Available: https://www.sciencedirect.com/science/article/pii/S0191261510001372

[26] H. Xiao, D. Zhu, and A. T. Chronopoulos, "Power allocation with energy efficiency optimization in cellular d2d-based v2x communication network," *IEEE Transactions on Intelligent Transportation Systems*, vol. 21, no. 12, pp. 4947–4957, Dec 2020.

[27] R. Yin, Y. Zhang, F. Dong, A. Wang, and C. Yuen, "Energy efficiency optimization in lte-u based small cell networks," *IEEE Transactions on Vehicular Technology*, vol. 68, no. 2, pp. 1963–1967, Feb 2019.

[28] P. Qin, Y. Fu, X. Feng, X. Zhao, S. Wang, and Z. Zhou, "Energy efficient resource allocation for parked cars based cellular-v2v heterogeneous networks," *IEEE Internet of Things Journal*, pp. 1–1, 2021.

[29] X. Wu, Z. Ma, X. Chen, F. Labeau, and S. Han, "Energy efficiency-aware joint resource allocation and power allocation in multi-user beamforming," *IEEE Transactions on Vehicular Technology*, vol. 68, no. 5, pp. 4824–4833, May 2019.

[30] Y. Zhang, H. Zhang, and K. Long, "Energy efficient resource allocation in cache based terahertz vehicular networks: A mean-field game approach," *IEEE Transactions on Vehicular Technology*, vol. 70, no. 6, pp. 5275–5285, June 2021.

[31] S. Lim and H. Kim, "Improving information age in sae j2945 congestion-controlled beaconing," *IEEE Communications Letters*, vol. 23, no. 2, pp. 358–361, Feb 2019.

[32] J. Aznar-Poveda, A.-J. Garcia-Sanchez, E. Egea-Lopez, and J. Garcia-Haro, "Mdprp: A q-learning approach for the joint control of beaconing rate and transmission power in vanets," *IEEE Access*, vol. 9, pp. 10 166–10 178, 2021.

[33] A. Hisham, D. Yuan, E. G. Ström, and F. Brännström, "Adjacent channel interference aware joint scheduling and power control for v2v broadcast communication," *IEEE Transactions on Intelligent Transportation Systems*, vol. 22, no. 1, pp. 443–456, Jan 2021.

[34] S. Samarakoon, M. Bennis, W. Saad, and M. Debbah, "Distributed federated learning for ultra-reliable low-latency vehicular communications," *IEEE Transactions on Communications*, vol. 68, no. 2, pp. 1146–1159, Feb 2020.

[35] A. Bazzi, A. Zanella, G. Cecchini, and B. M. Masini, "Analytical investigation of two benchmark resource allocation algorithms for lte-v2v," *IEEE Transactions on Vehicular Technology*, vol. 68, no. 6, pp. 5904–5916, June 2019.

[36] Y. Yan, J. Zhou, D. Tian, X. Duan, Z. Sheng, G. Qu, Y. Wu, and X. Ran, "Joint optimization of broadcast frequency and transmission power for lte-v2v based cooperative awareness of connected vehicles," in *2021 IEEE International Conference on Unmanned Systems (ICUS)*, 2021, pp. 390–395.

[37] G. Yang and M. Bai, "An optimized algorithm for power and beacon control in vanets based on ddpg," in *2021 IEEE International Conference on Consumer Electronics and Computer Engineering (ICCECE)*, Jan 2021, pp. 408–412.

[38] F. Goudarzi, H. Asgari, H. Al-Raweshidy, and E. Peytchev, "Joint beacon power and rate control for vehicular ad hoc networks," in *2019 IEEE SmartWorld, Ubiquitous Intelligence Computing, Advanced Trusted Computing, Scalable Computing Communications, Cloud Big Data Computing, Internet of People and Smart City Innovation (SmartWorld/SCALCOM/UIC/ATC/CBDCom/IOP/SCI)*, Aug 2019, pp. 1377–1383.

[39] J. Garbiso, A. Diaconescu, M. Coupechoux, and B. Leroy, "Fair self-adaptive clustering for hybrid cellular-vehicular networks," *IEEE Transactions on Intelligent Transportation Systems*, vol. 22, no. 2, pp. 1225–1236, Feb 2021.

[40] P. Li, L. Han, S. Xu, D. O. Wu, and P. Gong, "Resource allocation for 5g-enabled vehicular networks in unlicensed frequency bands," *IEEE Transactions on Vehicular Technology*, vol. 69, no. 11, pp. 13 546–13 555, Nov 2020.

[41] F. Goudarzi and H. Asgari, "Non-cooperative beacon power control for vanets," *IEEE Transactions on Intelligent Transportation Systems*, vol. 20, no. 2, pp. 777–782, Feb 2019.

[42] J. Zhou, D. Tian, Z. Sheng, X. Duan, and X. Shen, "Distributed task offloading optimization with queueing dynamics in multiagent mobile-edge computing networks," *IEEE Internet of Things Journal*, vol. 8, no. 15, pp. 12 311–12 328, Aug 2021.

[43] F. Zabini, A. Bazzi, B. M. Masini, and R. Verdone, "Optimal performance versus fairness tradeoff for resource allocation in wireless systems," *IEEE Transactions on Wireless Communications*, vol. 16, no. 4, pp. 2587–2600, 2017.

[44] Y. P. Fallah, N. Nasiriani, and H. Krishnan, "Stable and fair power control in vehicle safety networks," *IEEE Transactions on Vehicular Technology*, vol. 65, no. 3, pp. 1662–1675, March 2016.

[45] 3GPP, TS 33.885, "Universal mobile telecommunications system (umts); lte; architecture enhancements for v2x services, rel-14 v14.2.0," May 2017.

[46] 3GPP, TS 36.213, "Evolved universal terrestrial radio access (e-utra); physical layer procedures, rel-14 v14.3.0," June 2017.

[47] 3GPP, TS 36.355, "Evolved universal terrestrial radio access (e-utra); lte positioning protocol (lpp), rel-14 v14.2.0," June 2017.

[48] 3GPP, TS 36.171, "Evolved universal terrestrial radio access (e-utra); requirements for support of assisted global navigation satellite system (a-gnss), rel-13 v13.0.0," March 2017.

[49] Alcatel-Lucent, Alcatel-Lucent Shanghai Bell, "Utdoa performance with srs interference cancellation," Nov 2010.

[50] Y. Zhang, D. Niyato, and P. Wang, "Offloading in mobile cloudlet systems with intermittent connectivity," *IEEE Transactions on Mobile Computing*, vol. 14, no. 12, pp. 2516–2529, Dec 2015.

[51] F. Baccelli, B. Blaszczyszyn, and P. Muhlethaler, "An aloha protocol for multihop mobile wireless networks," *IEEE Transactions on Information Theory*, vol. 52, no. 2, pp. 421–436, Feb 2006.

[52] F. Bai and B. Krishnamachari, "Spatio-temporal variations of vehicle traffic in vanets: Facts and implications," in *Proceedings of the Sixth ACM International Workshop on VehiculAr InterNETworking*, ser. VANET '09. New York, NY, USA: Association for Computing Machinery, 2009, p. 43–52. [Online]. Available: https://doi.org/10.1145/1614269.1614278

[53] J. Haddad and A. Shraiber, "Robust perimeter control design for an urban region," *Transportation Research Part B: Methodological*, vol. 68, pp. 315–332, 2014. [Online]. Available: https://www.sciencedirect.com/science/article/pii/S0191261514001179

[54] J. Haddad and N. Geroliminis, "On the stability of traffic perimeter control in two-region urban cities," *Transportation Research Part B: Methodological*, vol. 46, no. 9, pp. 1159–1176, 2012. [Online]. Available: https://www.sciencedirect.com/science/article/pii/S0191261512000641

[55] R. Mohajerpoor, M. Saberi, H. L. Vu, T. M. Garoni, and M. Ramezani, "$\mathcal{H}^\infty$ robust perimeter flow control in urban networks with partial information feedback," *Transportation Research Part B: Methodological*, vol. 137, pp. 47–73, 2020, advances in Network Macroscopic Fundamental Diagram (NMFD) Research. [Online]. Available: https://www.sciencedirect.com/science/article/pii/S0191261518308609

[56] Y. Wan, J. Cao, W. Huang, J. Guo, and Y. Wei, "Perimeter control of multiregion urban traffic networks with time-varying delays," *IEEE Transactions on Systems, Man, and Cybernetics: Systems*, vol. 50, no. 8, pp. 2795–2803, Aug 2020.

[57] T. Lei, Z. Hou, and Y. Ren, "Data-driven model free adaptive perimeter control for multi-region urban traffic networks with route choice," *IEEE Transactions on Intelligent Transportation Systems*, vol. 21, no. 7, pp. 2894–2905, July 2020.

[58] D. Li and Z. Hou, "Perimeter control of urban traffic networks based on model-free adaptive control," *IEEE Transactions on Intelligent Transportation Systems*, pp. 1–13, 2020.

[59] S. F. A. Batista, D. Ingole, L. Leclercq, and M. Menéndez, "The role of trip lengths calibration in model-based perimeter control strategies," *IEEE Transactions on Intelligent Transportation Systems*, pp. 1–11, 2021.

[60] I. I. Sirmatel and N. Geroliminis, "Nonlinear moving horizon estimation for large-scale urban road networks," *IEEE Transactions on Intelligent Transportation Systems*, vol. 21, no. 12, pp. 4983–4994, Dec 2020.

[61] Y. Bichiou, M. Elouni, H. M. Abdelghaffar, and H. A. Rakha, "Sliding mode network perimeter control," *IEEE Transactions on Intelligent Transportation Systems*, vol. 22, no. 5, pp. 2933–2942, May 2021.

[62] Q. Chen, C. An, J. Xia, W. Rao, and S. Li, "Feedback linearization-based perimeter controllers for oversaturated regions," *IEEE Intelligent Transportation Systems Magazine*, pp. 0–0, 2020.

[63] J. Haddad, M. Ramezani, and N. Geroliminis, "Cooperative traffic control of a mixed network with two urban regions and a freeway," *Transportation Research Part B: Methodological*, vol. 54, pp. 17–36, 2013. [Online]. Available: https://www.sciencedirect.com/science/article/pii/S0191261513000477

[64] M. A. Patterson and A. V. Rao, "Gpops-ii: A matlab software for solving multiple-phase optimal control problems using hp-adaptive gaussian quadrature collocation methods and sparse

nonlinear programming," *ACM Trans. Math. Softw.*, vol. 41, no. 1, Oct. 2014. [Online]. Available: https://doi.org/10.1145/2558904

[65] M. Herceg, M. Kvasnica, C. Jones, and M. Morari, "Multi-Parametric Toolbox 3.0," in *Proc. of the European Control Conference*, Zürich, Switzerland, July 17–19 2013, pp. 502–510, http://control.ee.ethz.ch/~mpt.

[66] A. Bemporad, N. L. Ricker, and M. Morari, *Model Predic Control Toolbox User's Guide*.   U.S.: The MathWorks, Inc., 2021.

[67] L. Zhang, T. M. Garoni, and J. de Gier, "A comparative study of macroscopic fundamental diagrams of arterial road networks governed by adaptive traffic signal systems," *Transportation Research Part B: Methodological*, vol. 49, pp. 1–23, 2013. [Online]. Available: https://www.sciencedirect.com/science/article/pii/S0191261512001555

[68] 3GPP, TR 36.942, "Evolved universal terrestrial radio access (e-utra); radio frequency (rf) system scenarios, rel-14 v14.0.0," Mar. 2017.

Xuting Duan received the Ph.D. degree in traffic information engineering and control from Beihang University, Beijing, China, in 2017. He is currently an assistant professor with the School of Transportation Science and Engineering, Beihang University, Beijing, China. His current research interests are focused on vehicular ad hoc networks.

Yong Liang Guan [M'99-SM'10] received the Ph.D. degree from Imperial College London, U.K., and the Bachelor of Engineering degree (Hons.) from the National University of Singapore. He is currently a Professor of communication engineering with the School of Electrical and Electronic Engineering, Nanyang Technological University (NTU), where he leads the Continental-NTU Corporate Research Laboratory and the successful deployment of the campus-wide NTU-NXP V2X Testbed. His research interests broadly include coding and signal processing for communication systems and data storage systems. He is an Editor for IEEE Transactions on Vehicular Technology.

Jianshan Zhou received the B.Sc., M.Sc., and Ph.D. degrees in traffic information engineering and control from Beihang University, Beijing, China, in 2013, 2016, and 2020, respectively. He is an associate professor with the School of Transportation Science and Engineering at Beihang University. His research interests include vehicular communication networks, air-ground cooperative networks, connected autonomous vehicles, and intelligent transportation systems.

Victor C. M. Leung [S'75-M'89-SM'97-F'03] is a Distinguished Professor of Computer Science and Software Engineering at Shenzhen University, Shenzhen, China, and a Professor Emeritus at the University of British Columbia (UBC), Vancouver, Canada. Before he retired from UBC at the end of 2018, he was a Professor of Electrical and Computer Engineering and holder of the TELUS Mobility Research Chair there. His research is in the broad areas of wireless networks and mobile systems. He has coauthored more than 1300 journal/conference papers and book chapters. Dr. Leung is serving on the editorial boards of the IEEE Transactions on Green Communications and Networking, IEEE Transactions on Cloud Computing, IEEE Access, IEEE Network, and several other journals. He received the IEEE Vancouver Section Centennial Award, 2011 UBC Killam Research Prize, 2017 Canadian Award for Telecommunications Research, and 2018 IEEE TCGCC Distinguished Technical Achievement Recognition Award. He co-authored papers that won the 2017 IEEE ComSoc Fred W. Ellersick Prize, 2017 IEEE Systems Journal Best Paper Award, 2018 IEEE CSIM Best Journal Paper Award, and 2019 IEEE TCGCC Best Journal Paper Award. He is a Fellow of IEEE, the Royal Society of Canada, Canadian Academy of Engineering, and Engineering Institute of Canada. He is named in the current Clarivate Analytics list of "Highly Cited Researchers".

Guixian Qu received the B.Sc. degree in transportation engineering from Shandong University of Technology, Shandong, China, in 2012, the M.Sc. and Ph.D. degrees from Beijing University of Technology, Beijing, China, in 2014 and 2019, respectively. She is currently an Research Fellow of Research Institute of Aero-Engine, Beihang University. Her research interests include unmanned systems, dynamics modeling and control, and distributed optimization.

Daxin Tian [M'13-SM'16] received the Ph.D. degree in computer science from Jilin University, Changchun, China, in 2007. He is currently a University Professor with the School of Transportation Science and Engineering, Beihang University, Beijing, China. His research focuses on mobile computing, intelligent transportation systems, vehicular ad hoc networks, and swarm intelligent.

Zhengguo Sheng [SM'18] received the B.Sc. degree from the University of Electronic Science and Technology of China, Chengdu, China, in 2006, and the M.S. and Ph.D. degrees from Imperial College London, London, U.K., in 2007 and 2011, respectively. He is currently a Senior Lecturer with the University of Sussex, Brighton, U.K. His research interests cover IoT, vehicular communications, and cloud/edge computing.

Supplementary Material for
Joint Energy-Efficiency Communication Optimization and Perimeter Traffic Flow Control for Multi-Region LTE-V2V Networks

Jianshan Zhou, Guixian Qu, Daxin Tian, *Senior Member, IEEE,* Zhengguo Sheng, *Senior Member, IEEE,* Xuting Duan, Yong Liang Guan, *Senior Member, IEEE,* and Victor C. M. Leung, *Life Fellow, IEEE*

✦

APPENDIX A
ADDITIONAL LITERATURE REVIEW

Considerable studies have developed various EE optimization approaches based on convex approximation, mixed integer programming, and learning-based optimization [1]–[5]. In their system optimization models, EE objective as one of the important key performance indicators (KPIs) is usually defined as the transmission data rate achieved by consuming per unit power, which involves transmission power and data rate or beacon rate as key decision variables. Thus, many EE optimization models in the recent literature focus on power and rate control. For example, [6] considers the competitive behavior of vehicular users and proposes a non-cooperative game-theoretical approach to adapt power and beacon rate. In [7], the authors focus on a congested cross-road scenario and combine a k-means clustering algorithm with power allocation for cooperative vehicular communications. In [8], the authors develop a joint optimization framework that integrates electric vehicles' wireless charging, power allocation, and RB assignment to improve the EE performance of cellular V2X networks. [9] aims to optimize the capacity of NOMA-based V2X networks. The researchers combine graph theory and game theory to design a two-stage scheme to control vehicular users' power

- *Jianshan Zhou, Daxin Tian, and Xuting Duan are with State Key Lab of Intelligent Transportation System, Beijing Key Laboratory for Cooperative Vehicle Infrastructure Systems & Safety Control, the School of Transportation Science and Engineering, Beihang University, Beijing 100191, China (e-mail: jianshanzhou@foxmail.com, dtian@buaa.edu.cn, duanxuting@buaa.edu.cn).*
- *Guixian Qu is with the Aero-engine System Collaborative Design Center, Research Institute of Aero-Engine, Beihang University, Beijing 100191, China (e-mail: guixianqu@foxmail.com).*
- *Zhengguo Sheng is with the Department of Engineering and Design, University of Sussex, Richmond 3A09, UK (e-mail: z.sheng@sussex.ac.uk).*
- *Yong Liang Guan is with the School of Electrical and Electronic Engineering, Nanyang Technological University, Block S1-B1c-106, Nanyang Avenue, 639798, Singapore. (Email: eylguan@ntu.edu.sg).*
- *Victor C. M. Leung is with Department of Electrical and Computer Engineering, the University of British Columbia, Vancouver, B.C., V6T 1Z4 Canada (e-mail: vleung@ieee.org).*

(Corresponding author: Guixian Qu)

in a centralized and distributed manner, respectively [9]. Besides, [10] proposes an altruistic short-term prediction scheme to estimate local vehicle density in the coverage of a vehicle and develops a congestion control protocol via power and rate adaption using the density prediction. Due to the high mobility of vehicles, vehicular wireless channels are time-varying and in the presence of uncertainties. In this regard, some researchers focus on robust power optimization [11], [12], developing a statistical leaning algorithm to estimate the channel uncertainties and exploit the second-order cone programming technique to minimize the transmission power under the uncertainty set. In addition to power control, adaptive beaconing approaches have been investigated in the current literature. In this direction, the beaconing rate is adjusted according to the estimated channel load [13] or the channel's congestion degree [14]. In [15], the authors employ different preambles to design a distributed and adaptive reservation-based MAC protocol, allowing them to reserve resources, detect beacon collisions, and handle collisions to improve the reliability of vehicular beaconing. In some studies [16], [17], highly accurate time synchronization and positioning algorithms are applied to enhance vehicular beaconing applications. The above studies show success in improving the performance of vehicular networks at a microscopic scale. However, considering large-scale deployment in a city, they need to touch on the critical problem of optimizing the communication networks at a macroscopic scale, a spatial aggregation scale, regarding the macroscopic traffic flow dynamics of the city.

Macroscopic traffic dynamics modeling and control is crucial in managing large-scale road traffic networks within urban areas and has garnered increasing attention from the transportation community. Many research endeavors have been dedicated to macroscopic traffic control, particularly developing advanced perimeter control approaches utilizing macroscopic fundamental diagrams (MFDs) in urban areas [18]–[33]. The theoretical proposition of MFD is originally presented in [34] and verified by using simulated or empirical data collected from real urban cities such as Yokohama, Japan [35]–[37]. The MFD is introduced to model

the aggregated traffic flow dynamics in multiple urban regions. It describes the relationship between multi-region space-mean flows (or outflows defined by trip completion flows from the regions) and vehicle densities evolving over time. While many existing studies have shown a significant advance in designing and applying various MFD-based perimeter flow control approaches to balance traffic load distribution over multiple adjacent regions and relieve traffic congestion, their solutions do not cope with the issue of vehicular communication and networking. In the transportation community, few research efforts are made on joint vehicular communication optimization and macroscopic traffic control from multi-disciplinary perspectives.

APPENDIX B
PROOF OF LEMMA 1

From (33), it is seen that $\widetilde{\mathcal{L}}_\sigma(\mathcal{F}, \mathcal{P}, \mathcal{Z}, \boldsymbol{\lambda})$ is continuously differentiable with respect to the nonnegative slack variables $\mathcal{Z}$. Thus, even though $V(\mathcal{F}, \mathcal{P})$ is not smooth and its gradient and Hessian matrix may not be available, the gradient of $\widetilde{\mathcal{L}}_\sigma(\mathcal{F}, \mathcal{P}, \mathcal{Z}, \boldsymbol{\lambda})$ with respect to $\mathcal{Z}$ always exists. At this point, in order to determine an locally optimal $\mathcal{Z}$, we can let $\nabla_{\mathcal{Z}} \widetilde{\mathcal{L}}_\sigma(\mathcal{F}, \mathcal{P}, \mathcal{Z}, \boldsymbol{\lambda}) = \mathbf{0}$ according to the well-known first-order optimality conditions, i.e., the Karush-Kuhn-Tucker (KKT) conditions, from which we further derive

$$
\begin{aligned}
&z_{l,i}(k)\left[\lambda_{l,i}(k) - \sigma\left(\mu_{l,i}(k) - z_{l,i}^2(k)\right)\right] \\
&= z_{l,i}(k)\left[\sigma z_{l,i}^2(k) - (\sigma\mu_{l,i}(k) - \lambda_{l,i}(k))\right] = 0
\end{aligned}
\tag{S.1}
$$

for all $l = 1, \ldots, 4$; $i \in \mathcal{N}$; $k \in \mathcal{K}$. (S.1) can indicate two specific cases as follows:

i) If $\sigma\mu_{l,i}(k) - \lambda_{l,i}(k) \geq 0$, the optimum is attained at

$$
z_{l,i}^2(k) = \frac{\sigma\mu_{l,i}(k) - \lambda_{l,i}(k)}{\sigma}, \; l = 1, \ldots, 4; \; i \in \mathcal{N}; \; k \in \mathcal{K}.
\tag{S.2}
$$

ii) If $\sigma\mu_{l,i}(k) - \lambda_{l,i}(k) < 0$, it is seen that

$$
\sigma z_{l,i}^2(k) \neq (\sigma\mu_{l,i}(k) - \lambda_{l,i}(k)), \; l = 1, \ldots, 4; \; i \in \mathcal{N}; \; k \in \mathcal{K}.
\tag{S.3}
$$

At this point, the optimum must be $z_{l,i}(k) = 0$ for all $l = 1, \ldots, 4$; $i \in \mathcal{N}$; $k \in \mathcal{K}$.

Combining both the above results can yield

$$
z_{l,i}^2(k) = \begin{cases} \frac{\sigma\mu_{l,i}(k) - \lambda_{l,i}(k)}{\sigma}, & \sigma\mu_{l,i}(k) \geq \lambda_{l,i}(k); \\ 0, & \text{otherwise.} \end{cases}
\tag{S.4}
$$

Substituting (S.4) into $\widetilde{\mathcal{L}}_\sigma(\mathcal{F}, \mathcal{P}, \mathcal{Z}, \boldsymbol{\lambda})$ derives $\mathcal{L}_\sigma(\mathcal{F}, \mathcal{P}, \boldsymbol{\lambda})$ as in (34) along with (35). Hence, the lemma is proven.

APPENDIX C
PROOF OF LEMMA 2

The sufficiency in Lemma 2 immediately follows the given condition $\boldsymbol{B}^{\mathrm{T}}\boldsymbol{x} = \mathbf{0}$. That is, we can see $\sigma\boldsymbol{x}^{\mathrm{T}}\boldsymbol{B}\boldsymbol{B}^{\mathrm{T}}\boldsymbol{x} = \mathbf{0}$ for any $\sigma \geq \sigma^*$, which can lead to

$$
\boldsymbol{x}^{\mathrm{T}}\boldsymbol{A}\boldsymbol{x} = \boldsymbol{x}^{\mathrm{T}}(\boldsymbol{A} + \sigma\boldsymbol{B}\boldsymbol{B}^{\mathrm{T}})\boldsymbol{x} > 0.
\tag{S.5}
$$

Next, we first show the conditional necessity. That is, assuming that there exists a positive $\sigma^* > 0$ satisfying

$\boldsymbol{x}^{\mathrm{T}}(\boldsymbol{A} + \sigma^*\boldsymbol{B}\boldsymbol{B}^{\mathrm{T}})\boldsymbol{x} > 0$ for any non-zero $\boldsymbol{x} \neq \mathbf{0}$, $\boldsymbol{x} \in \mathbb{R}^{n \times 1}$, we can easily see

$$
\boldsymbol{x}^{\mathrm{T}}(\boldsymbol{A} + \sigma\boldsymbol{B}\boldsymbol{B}^{\mathrm{T}})\boldsymbol{x} \geq \boldsymbol{x}^{\mathrm{T}}(\boldsymbol{A} + \sigma^*\boldsymbol{B}\boldsymbol{B}^{\mathrm{T}})\boldsymbol{x} > 0
\tag{S.6}
$$

holds true for all $\sigma \geq \sigma^*$.

To prove the overall necessity, we only need to prove the existence of σ^* as stated above. For this goal, we present a proof by mathematical contradiction as follows. we suppose that such a σ^* does not exist and thus there must exist a non-zero column vector $\boldsymbol{y}_k \neq \mathbf{0}$, $\boldsymbol{y}_k \in \mathbb{R}^{n \times 1}$ such that $\boldsymbol{y}_k^{\mathrm{T}}(\boldsymbol{A} + k\boldsymbol{B}\boldsymbol{B}^{\mathrm{T}})\boldsymbol{y}_k \leq 0$, i.e.,

$$
\frac{\boldsymbol{y}_k^{\mathrm{T}}}{\|\boldsymbol{y}_k\|}(\boldsymbol{A} + k\boldsymbol{B}\boldsymbol{B}^{\mathrm{T}})\frac{\boldsymbol{y}_k}{\|\boldsymbol{y}_k\|} \leq 0,
\tag{S.7}
$$

for any a positive integer $k \in \mathbb{Z}_{>0}$.

It is recognized that $\|(\boldsymbol{y}_k/\|\boldsymbol{y}_k\|)\| = 1$. Hence, this fact indicates that $\{\boldsymbol{y}_k/\|\boldsymbol{y}_k\|, \forall k \in \mathbb{Z}_{>0}\}$ is a bounded sequence. According to the Bolzano-Weierstrass' theorem that any bounded sequence must have a convergent subsequence, we denote a convergent subsequence derived from $\{\boldsymbol{y}_k/\|\boldsymbol{y}_k\|, \forall k \in \mathbb{Z}_{>0}\}$ by $\{\boldsymbol{x}_{k_i}, k_i \in \mathbb{Z}_{>0}\}$ and its limit by $\bar{\boldsymbol{x}}$, i.e., $\lim_{k_i \to \infty} \boldsymbol{x}_{k_i} = \bar{\boldsymbol{x}}$ and $\|\bar{\boldsymbol{x}}\| = 1$. Similar to (S.7), for such a convergent subsequence $\{\boldsymbol{x}_{k_i}, k_i \in \mathbb{Z}_{>0}\}$, we have

$$
\boldsymbol{x}_{k_i}^{\mathrm{T}}(\boldsymbol{A} + k_i\boldsymbol{B}\boldsymbol{B}^{\mathrm{T}})\boldsymbol{x}_{k_i} \leq 0.
\tag{S.8}
$$

Moreover, taking the limit on both sides of (S.8) under $k_i \to \infty$ can yield

$$
\begin{aligned}
&\bar{\boldsymbol{x}}^{\mathrm{T}}\boldsymbol{A}\bar{\boldsymbol{x}} + \lim_{k_i \to \infty} k_i\left(\boldsymbol{B}^{\mathrm{T}}\boldsymbol{x}_{k_i}\right)^{\mathrm{T}}\boldsymbol{B}^{\mathrm{T}}\boldsymbol{x}_{k_i} \\
&= \bar{\boldsymbol{x}}^{\mathrm{T}}\boldsymbol{A}\bar{\boldsymbol{x}} + k_i\left\|\boldsymbol{B}^{\mathrm{T}}\boldsymbol{x}_{k_i}\right\|_2^2 \leq 0.
\end{aligned}
\tag{S.9}
$$

Since the term $\bar{\boldsymbol{x}}^{\mathrm{T}}\boldsymbol{A}\bar{\boldsymbol{x}}$ is deterministic, we can have $\lim_{k_i \to \infty} \boldsymbol{B}^{\mathrm{T}}\boldsymbol{x}_{k_i} = \boldsymbol{B}^{\mathrm{T}}\bar{\boldsymbol{x}} = \mathbf{0}$. Otherwise, if $\boldsymbol{B}^{\mathrm{T}}\bar{\boldsymbol{x}} \neq \mathbf{0}$, we would see $\lim_{k_i \to \infty} k_i\boldsymbol{x}_{k_i}^{\mathrm{T}}\boldsymbol{B}\boldsymbol{B}^{\mathrm{T}}\boldsymbol{x}_{k_i} = k_i\|\boldsymbol{B}^{\mathrm{T}}\bar{\boldsymbol{x}}\|_2^2 \to \infty$, which is contradictory with (S.9). Combining $\boldsymbol{B}^{\mathrm{T}}\bar{\boldsymbol{x}} = \mathbf{0}$ and (S.9) also leads to $\bar{\boldsymbol{x}}^{\mathrm{T}}\boldsymbol{A}\bar{\boldsymbol{x}} \leq 0$, which is contradictory with the condition of the theorem. At this point, the contradiction occurs. Therefore, the existence of σ^* holds true and the overall lemma is proven.

APPENDIX D
PROOF OF THEOREM 1

At the continuously twice-differentiable feasible points, we can derive the gradient of $\widetilde{\mathcal{L}}_\sigma(\mathcal{F}, \mathcal{P}, \mathcal{Z}^*, \boldsymbol{\lambda}^*)$ with respect to $\mathcal{F}$ and $\mathcal{P}$ as follows

$$
\nabla_{\mathcal{S}}\widetilde{\mathcal{L}}_\sigma(\mathcal{F}, \mathcal{P}, \mathcal{Z}^*, \boldsymbol{\lambda}^*) = \nabla_{\mathcal{S}}\widetilde{\mathcal{L}}(\mathcal{F}, \mathcal{P}, \mathcal{Z}^*, \boldsymbol{\lambda}^*) + \sigma\Phi(\mathcal{S})\phi,
\tag{S.10}
$$

where $\mathcal{S}$ denotes $\mathcal{S} = \mathrm{col}\{\mathcal{F}, \mathcal{P}\}$, ϕ is a column vector as the collection of all $\phi_{l,i}(k)$, i.e., $\phi = \mathrm{col}\{\phi_{l,i}(k), l = 1, \ldots, 4; i \in \mathcal{N}; k \in \mathcal{K}\}$. $\Phi(\mathcal{S})$ is the gradient matrix of ϕ, i.e., $\Phi(\mathcal{S}) = (\nabla_{\mathcal{S}}\phi_{l,i}(k), l = 1, \ldots, 4; i \in \mathcal{N}; k \in \mathcal{K})$. According to the second-order sufficient optimality conditions of (32), the feasible $\mathcal{F}^*$ and $\mathcal{P}^*$ satisfy the constraints $\phi_{l,i}(k) = 0$ for all $l = 1, \ldots, 4$, $i \in \mathcal{N}$, and $k \in \mathcal{K}$, and also $\nabla_{\mathcal{S}}\widetilde{\mathcal{L}}(\mathcal{F}^*, \mathcal{P}^*, \mathcal{Z}^*, \boldsymbol{\lambda}^*) = \mathbf{0}$. Thus, we can see

$$
\nabla_{\mathcal{S}}\widetilde{\mathcal{L}}_\sigma(\mathcal{F}^*, \mathcal{P}^*, \mathcal{Z}^*, \boldsymbol{\lambda}^*) = \nabla_{\mathcal{S}}\widetilde{\mathcal{L}}(\mathcal{F}^*, \mathcal{P}^*, \mathcal{Z}^*, \boldsymbol{\lambda}^*) = \mathbf{0}.
\tag{S.11}
$$

In addition, based on (S.10), the Hessian of $\widetilde{\mathcal{L}}_\sigma\left(\mathcal{F}, \mathcal{P}, \mathcal{Z}^*, \boldsymbol{\lambda}^*\right)$ with respect to $\mathcal{F}$ and $\mathcal{P}$ is given by

$$
\begin{aligned}
\nabla_{\mathcal{S}}^2 \widetilde{\mathcal{L}}_\sigma\left(\mathcal{F}, \mathcal{P}, \mathcal{Z}^*, \boldsymbol{\lambda}^*\right) = {}& \nabla_{\mathcal{S}}^2 \widetilde{\mathcal{L}}\left(\mathcal{F}, \mathcal{P}, \mathcal{Z}^*, \boldsymbol{\lambda}^*\right) \\
& + \sigma \Phi(\mathcal{S}) \Phi(\mathcal{S})^{\mathrm{T}}.
\end{aligned}
\tag{S.12}
$$

According to the second-order sufficient optimality conditions of (32), it always holds

$$
\boldsymbol{s}^{\mathrm{T}} \nabla_{\mathcal{S}}^2 \widetilde{\mathcal{L}}\left(\mathcal{F}^*, \mathcal{P}^*, \mathcal{Z}^*, \boldsymbol{\lambda}^*\right) \boldsymbol{s} > 0
\tag{S.13}
$$

for any non-zero column vector $\boldsymbol{s} \neq \boldsymbol{0}$ with the compatible dimension of $\mathcal{S}^* = \mathrm{col}\{\mathcal{F}^*, \mathcal{P}^*\}$ and satisfying $\Phi(\mathcal{S}^*)^{\mathrm{T}} \boldsymbol{s} = \boldsymbol{0}$ at $\mathcal{F}^*, \mathcal{P}^*$. Now, using Lemma 2, we can further conclude that there must exist a positive $\sigma^* > 0$ such that $\mathcal{F}^*$ and $\mathcal{P}^*$ satisfy

$$
\begin{aligned}
\boldsymbol{s}^{\mathrm{T}} & \begin{pmatrix} \nabla_{\mathcal{S}}^2 \widetilde{\mathcal{L}}\left(\mathcal{F}^*, \mathcal{P}^*, \mathcal{Z}^*, \boldsymbol{\lambda}^*\right) \\ + \sigma \Phi(\mathcal{S}^*) \Phi(\mathcal{S}^*)^{\mathrm{T}} \end{pmatrix} \boldsymbol{s} \\
& = \boldsymbol{s}^{\mathrm{T}} \nabla_{\mathcal{S}}^2 \widetilde{\mathcal{L}}_\sigma\left(\mathcal{F}^*, \mathcal{P}^*, \mathcal{Z}^*, \boldsymbol{\lambda}^*\right) \boldsymbol{s} > 0
\end{aligned}
\tag{S.14}
$$

for any $\sigma \geq \sigma^*$. At this point, combining both the first-order and the second-order results of (S.11) and (S.14) can indicate that $\mathcal{F}^*$ and $\mathcal{P}^*$ also satisfy the second-order sufficient optimality conditions of (38). They are also a strict local minima of (38).

When a feasible $\bar{\mathcal{F}}$ and a feasible $\bar{\mathcal{P}}$ meet $\phi_{l,i}(k) = 0$ for all $l = 1, \ldots, 4, i \in \mathcal{N}, k \in \mathcal{K}$, and are a local minima of (39) for some specific $\bar{\mathcal{Z}}, \bar{\sigma} > 0$ and $\bar{\boldsymbol{\lambda}}$, we can have

$$
\begin{aligned}
V\left(\bar{\mathcal{F}}, \bar{\mathcal{P}}\right) &= \widetilde{\mathcal{L}}_{\bar{\sigma}}\left(\bar{\mathcal{F}}, \bar{\mathcal{P}}, \bar{\mathcal{Z}}, \bar{\boldsymbol{\lambda}}\right) \\
&\leq \widetilde{\mathcal{L}}_{\bar{\sigma}}\left(\mathcal{F}_0, \mathcal{P}_0, \bar{\mathcal{Z}}, \bar{\boldsymbol{\lambda}}\right) = V\left(\mathcal{F}_0, \mathcal{P}_0\right).
\end{aligned}
\tag{S.15}
$$

for any feasible point $\mathcal{F}_0$ and $\mathcal{P}_0$, which also satisfy $\phi_{l,i}(k) = 0$ for all $l = 1, \ldots, 4, i \in \mathcal{N}, k \in \mathcal{K}$, and are sufficiently closed to $\bar{\mathcal{F}}$ and $\bar{\mathcal{P}}$. The above result indicates that the the feasible $\bar{\mathcal{F}}$ and $\bar{\mathcal{P}}$ are a local minima of (32). At this point, the overall theorem is proven.

APPENDIX E
PROOF OF THEOREM 2

The theorem immediately follows Lemma 1 and Theorem 1. That is, Lemma 1 shows the equivalence of the problems (40) and (39). Thus, a local minimum of (40) is equivalent to that of (32) and the existence of σ^* is guaranteed according to Theorem 1.

APPENDIX F
PROOF OF THEOREM 3

According to Theorems 1 and 2, we can see that $V\left(\mathcal{F}^*, \mathcal{P}^*; \mathcal{U}^*\right) \leq V\left(\mathcal{F}, \mathcal{P}; \mathcal{U}^*\right)$ holds for any feasible $\mathcal{F}$ and $\mathcal{P}$ in (31) where $V\left(\mathcal{F}, \mathcal{P}; \mathcal{U}^*\right)$ is used to denote the conditional objective function based on the perimeter control $\mathcal{U}^*$. Recalling $C\left(\mathcal{U}^*\right) < C\left(\mathcal{U}\right)$ and the definition of the Pareto optimality in (28), we can prove the theorem by contradiction. That is, if there exist such a feasible perimeter control $\widetilde{\mathcal{U}}, \widetilde{\mathcal{U}} \neq \mathcal{U}^*$, such that it can improve the objective of the model (31), i.e., $V\left(\mathcal{F}^*, \mathcal{P}^*; \mathcal{U}^*\right) > V\left(\mathcal{F}, \mathcal{P}; \widetilde{\mathcal{U}}\right)$. On the other side, it will also impair the objective of the model

(30) and does not hold the optimality for (30), i.e., there exist some feasible $\mathcal{U}$ such that $C\left(\widetilde{\mathcal{U}}\right) \geq C\left(\mathcal{U}\right)$. At this point, the Pareto optimal solution must contain $\mathcal{U}^*$. Since $\{\mathcal{F}^*, \mathcal{P}^*\}$ are obtained dependent on $\mathcal{U}^*$, $\{\mathcal{F}^*, \mathcal{P}^*, \mathcal{U}^*\}$ is a Pareto-optimal solution where no individual objective can be better off without making the other individual objective worse off. Thus, the theorem can be proven.

APPENDIX G
FORMULATION OF JAIN'S FAIRNESS INDEX

Jain's fairness index is a widely known metric used for evaluating the fairness of resource allocation among different users or systems. In the simulation experiment, we refer to the fairness index to quantify the EE performance distribution over different urban regions. This performance metric denoted by FI is formulated as follows

$$
FI = \frac{\left(\sum_{i \in \mathcal{N}} J_i\left(x_i(t), f_i(t), p_i(t)\right)\right)^2}{N \sum_{i \in \mathcal{N}} \left(J_i\left(x_i(t), f_i(t), p_i(t)\right)\right)^2},
\tag{S.16}
$$

where $J_i\left(x_i(t), f_i(t), p_i(t)\right)$ is the achievable EE performance metric of the region $i \in \mathcal{N}$.

APPENDIX H
ADDITIONAL VALIDATION AND COMPARISON

This supplementary material provides more simulation results to validate the proposed joint vehicular communication optimization and macroscopic traffic control (VCOMTC) method. We test its ability to balance the temporal-spatial traffic flow distribution over multiple regions meanwhile improving the global energy-efficiency (EE) performance of the LTE-V2V networks in these regions, using another different scenario configuration. Specifically, we change the MFDs and the time-varying macroscopic traffic demands of a three-region urban area and adopt the same configurations for other communication parameters as the main text. Figure 1 shows the MFD profile of each region, while Figure 2 illustrates their time-varying traffic demands. In particular, we decrease the peak-hour traffic demands of the region $i = 3$ to narrow the difference between the three regions' traffic demands. These configurations in Figure 1 and Figure 2 differ from those in the main text. Thus, we can examine the generality of the proposed method using the different configurations.

Figure 3 and Figure 4 show the transfer flow dynamics of the regions without and with the MPC-based perimeter control, respectively. It can be observed from Figure 3 that, even though the region $i = 3$ has similar traffic demands as the other two regions in Figure 2, it experiences much higher traffic accumulation than the regions and the total delay of the road traffic network is considerable. The sum of the vehicle accumulations of the region $i = 3$ exceeds the jam accumulation, i.e., 10^4 (veh), after about $4600\,\mathrm{s}$, while the other regions are free of traffic congestion. This result indicates a highly imbalanced traffic distribution over the regions when the regions do not adopt the proposed perimeter control approach. By comparison, when applying the MPC-based perimeter control, the three regions' vehicle accumulations can always be regulated in an uncongested
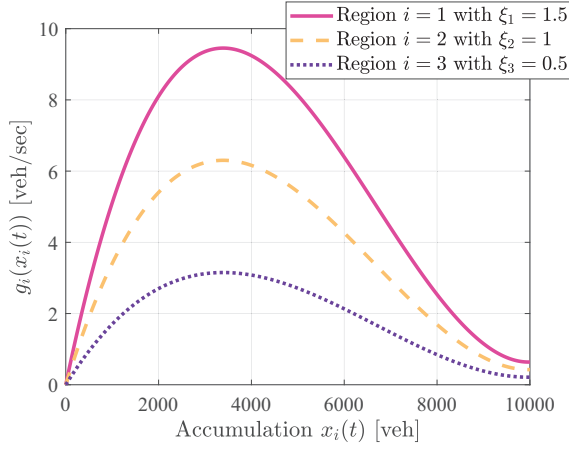
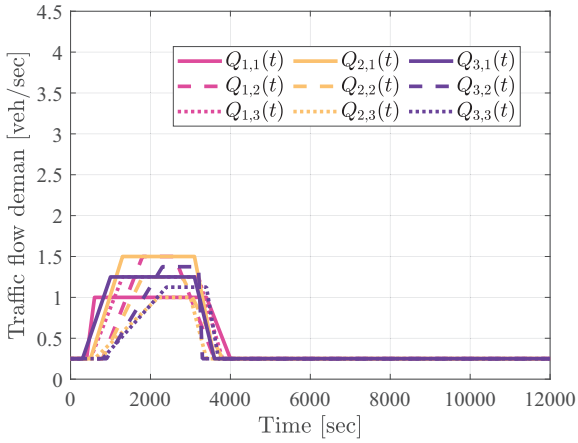Fig. 1. The MFDs of a three-region urban area.

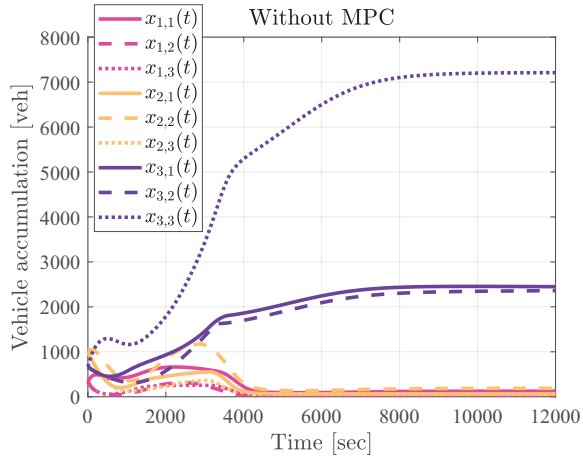Fig. 2. The time-varying traffic demands of the three urban regions.

Fig. 3. The dynamics of the transfer flows from each urban region without the MPC-based perimeter control.
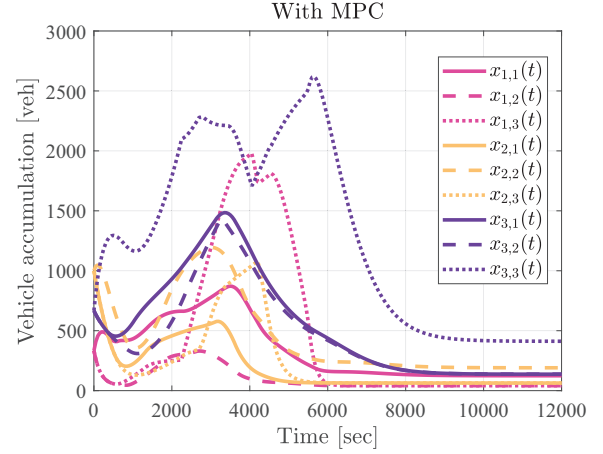

Fig. 4. The dynamics of the transfer flows from each urban region with the MPC-based perimeter control.

Moreover, we compare our proposed joint optimization and control method with the other baselines, the CCP and the ACP methods as detailed in the main text, and the advanced scheme, the VCO method, that uses the state-of-the-art constrained optimization methodology.[1] Figure 5 and Figure 6 demonstrate the EE performance of the LTE-V2V networks in the three regions using two different modulation and coding schemes (MCS), QPSK and 16-QAM, respectively. Our proposed method can provide the highest EE performance for all the regions on average among the methods. In particular, our method boosts the EE performance of the LTE-V2V network in the region $i = 3$ after about $6000\,\mathrm{s}$, while the network performance degrades under the VCO method. This is because the compared method cannot coordinate the multi-region traffic flow dynamics and cannot adapt communication optimization to the multi-region traffic dynamics. In the LTE-V2V networks of the regions, $i = 1, 2$, with low-level vehicle accumulations, our method provides similar EE performance to the VCO. However, for the region $i = 3$ with the heavy vehicle accumulation, the compared method makes the LTE resource blocks insufficient to support vehicular communications, increasing transmission collisions and packet loss. On the contrary, our method improves the EE performance of the LTE-V2V network in this dense region by more than 30% under the QPSK and the 16-QAM schemes, compared to the other methods. The result confirms the significant benefit of joint vehicular communication optimization and macroscopic traffic control.

In Figure 7, we show the system-level accumulated EE over the whole time horizon and observe that our method outperforms the others. Specifically, our method provides comparable EE performance to the VCO method under the

state. Figure 4 shows that our MPC-based perimeter controllers clear the regions' vehicle accumulations to reduce the total delay of the road traffic network, improving the temporal-spatial balance of the multi-region traffic dynamics and the macroscopic traffic efficiency.

---

1. To the best of our knowledge, no existing methodologies can directly address the scenario problem that couples the energy-efficiency optimization of multi-region LTE-V2V networks and the multi-region macroscopic traffic dynamics control. Thus, we treat an existing constrained optimization approach (i.e., the VCO), also based on the Lagrangian multiplier theory, as a state-of-the-art method for performance comparison. The VCO method is not driven by coordinated macroscopic traffic dynamics. Therefore, it does not incorporate multi-region perimeter control. The comparison with the VCO enables us to highlight the significance of joint optimization and control.
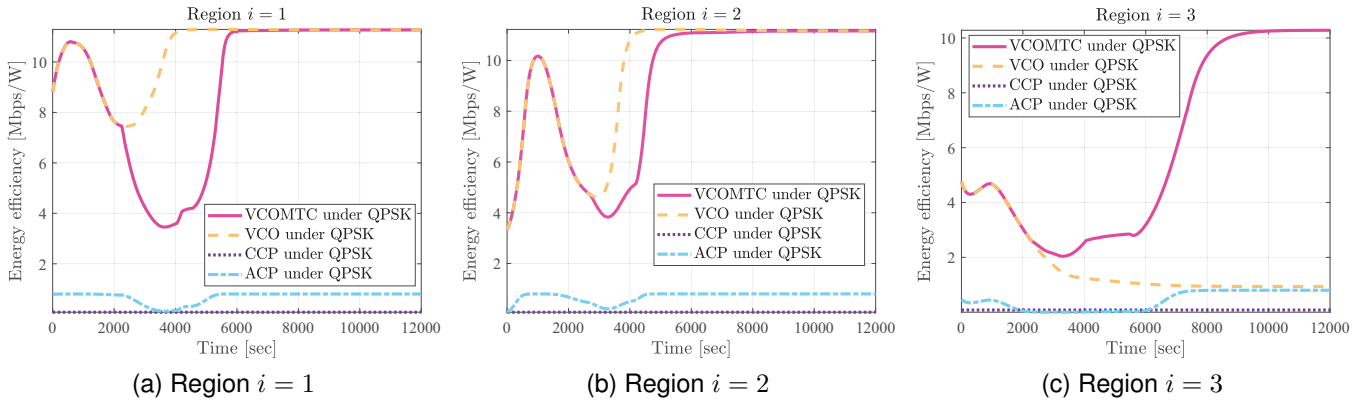
Fig. 5. The evolution of the multi-region EE metrics under comparative methods using the QPSK modulation scheme.
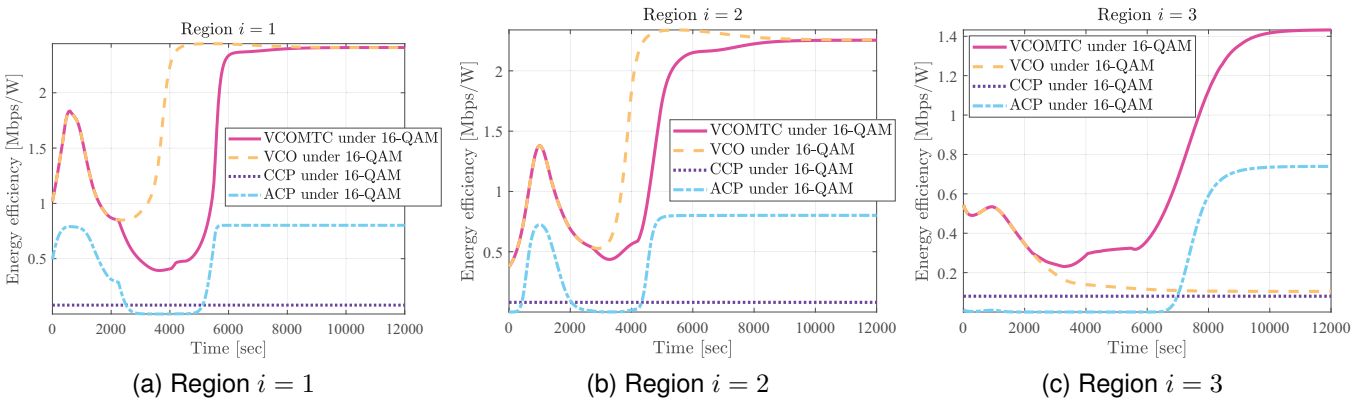

Fig. 6. The evolution of the multi-region EE metrics under comparative methods using the 16-QAM modulation scheme.

16-QAM scheme and achieves 10.49% higher EE performance than the compared method under the QPSK scheme. Figure 8 illustrates the LTE resource utilization fairness index among multiple regions. Our method can achieve fairer resource utilization on average than the VCO method as time evolves. Jain's fairness index of the VCO method is decreasing after 4000 s. By comparison, even though our method experiences a performance drop between 2500 s and 6000 s since the urban regions have high vehicle accumulations during this phase, it dramatically improves the fairness performance after that. Our method provides almost 100% fairness under the QPSK scheme and more than 95% under the 16-QAM finally. Overall, the multi-region LTE-V2V networks can better benefit from incorporating macroscopic traffic control into vehicular communication optimization. The above supplementary results validate our proposed method, proving the conclusions consistent with those in the main text.

Fig. 7. The system-level accumulated EE under comparative methods.

REFERENCES

[1] H. Xiao, D. Zhu, and A. T. Chronopoulos, "Power allocation with energy efficiency optimization in cellular d2d-based v2x communication network," *IEEE Transactions on Intelligent Transportation Systems*, vol. 21, no. 12, pp. 4947–4957, Dec 2020.

[2] R. Yin, Y. Zhang, F. Dong, A. Wang, and C. Yuen, "Energy efficiency optimization in lte-u based small cell networks," *IEEE Transactions on Vehicular Technology*, vol. 68, no. 2, pp. 1963–1967, Feb 2019.

[3] P. Qin, Y. Fu, X. Feng, X. Zhao, S. Wang, and Z. Zhou, "Energy efficient resource allocation for parked cars based cellular-v2v heterogeneous networks," *IEEE Internet of Things Journal*, pp. 1–1, 2021.

[4] X. Wu, Z. Ma, X. Chen, F. Labeau, and S. Han, "Energy efficiency-aware joint resource allocation and power allocation in multi-user beamforming," *IEEE Transactions on Vehicular Technology*, vol. 68,
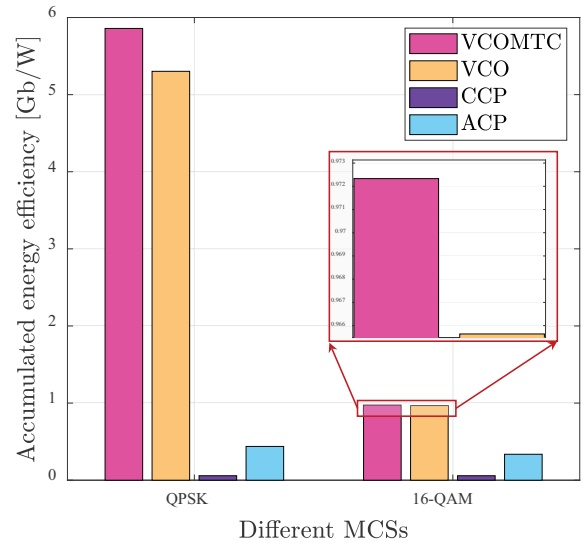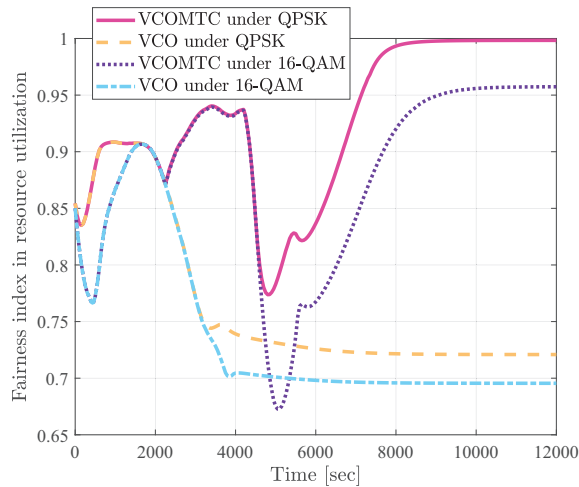
Fig. 8. The evolution of Jain's fairness index in resource utilization under comparative methods.

no. 5, pp. 4824–4833, May 2019.

[5] Y. Zhang, H. Zhang, and K. Long, "Energy efficient resource allocation in cache based terahertz vehicular networks: A mean-field game approach," *IEEE Transactions on Vehicular Technology*, vol. 70, no. 6, pp. 5275–5285, June 2021.

[6] F. Goudarzi and H. Asgari, "Non-cooperative beacon power control for vanets," *IEEE Transactions on Intelligent Transportation Systems*, vol. 20, no. 2, pp. 777–782, Feb 2019.

[7] H. Xiao, Y. Chen, Q. Zhang, A. T. Chronopoulos, Z. Zhang, and S. Ouyang, "Joint clustering and power allocation for the cross roads congestion scenarios in cooperative vehicular networks," *IEEE Transactions on Intelligent Transportation Systems*, vol. 20, no. 6, pp. 2267–2277, June 2019.

[8] F. Jameel, W. U. Khan, N. Kumar, and R. Jäntti, "Efficient power-splitting and resource allocation for cellular v2x communications," *IEEE Transactions on Intelligent Transportation Systems*, vol. 22, no. 6, pp. 3547–3556, June 2021.

[9] F. Zhang, M. M. Wang, X. Bao, and W. Liu, "Centralized resource allocation and distributed power control for noma-integrated nr v2x," *IEEE Internet of Things Journal*, vol. 8, no. 22, pp. 16 522–16 534, Nov 2021.

[10] S. Zemouri, S. Djahel, and J. Murphy, "An altruistic prediction-based congestion control for strict beaconing requirements in urban vanets," *IEEE Transactions on Systems, Man, and Cybernetics: Systems*, vol. 49, no. 12, pp. 2582–2597, Dec 2019.

[11] S. Zhang, J. Zhou, D. Tian, Z. Sheng, X. Duan, and V. C. M. Leung, "Robust cooperative communication optimization for multi-uav-aided vehicular networks," *IEEE Wireless Communications Letters*, vol. 10, no. 4, pp. 780–784, 2021.

[12] W. Wu, R. Liu, Q. Yang, H. Shan, and T. Q. S. Quek, "Learning-based robust resource allocation for ultra-reliable v2x communications," *IEEE Transactions on Wireless Communications*, vol. 20, no. 8, pp. 5199–5211, Aug 2021.

[13] F. Hajiaghajani and C. Qiao, "Tailgating risk-aware beacon rate adaptation for distributed congestion control in vanets," in *2019 IEEE Global Communications Conference (GLOBECOM)*, Dec 2019, pp. 1–6.

[14] F. Lyu, N. Cheng, H. Zhu, H. Zhou, W. Xu, M. Li, and X. Shen, "Towards rear-end collision avoidance: Adaptive beaconing for connected vehicles," *IEEE Transactions on Intelligent Transportation Systems*, vol. 22, no. 2, pp. 1248–1263, Feb 2021.

[15] H. Mosavat-Jahromi, Y. Li, Y. Ni, and L. Cai, "Distributed and adaptive reservation mac protocol for beaconing in vehicular networks," *IEEE Transactions on Mobile Computing*, vol. 20, no. 10, pp. 2936–2948, Oct 2021.

[16] J. A. Ansere, G. Han, and H. Wang, "A novel reliable adaptive beacon time synchronization algorithm for large-scale vehicular ad hoc networks," *IEEE Transactions on Vehicular Technology*, vol. 68, no. 12, pp. 11 565–11 576, Dec 2019.

[17] S. Bolufé, C. A. Azurdia-Meza, S. Céspedes, S. Montejo-Sánchez, R. D. Souza, and E. M. G. Fernandez, "Posacc: Position-accuracy based adaptive beaconing algorithm for cooperative vehicular safety systems," *IEEE Access*, vol. 8, pp. 15 484–15 501, 2020.

[18] J. Haddad and A. Shraiber, "Robust perimeter control design for an urban region," *Transportation Research Part B: Methodological*, vol. 68, pp. 315–332, 2014. [Online]. Available: https://www.sciencedirect.com/science/article/pii/S0191261514001179

[19] J. Haddad and N. Geroliminis, "On the stability of traffic perimeter control in two-region urban cities," *Transportation Research Part B: Methodological*, vol. 46, no. 9, pp. 1159–1176, 2012. [Online]. Available: https://www.sciencedirect.com/science/article/pii/S0191261512000641

[20] N. Geroliminis, J. Haddad, and M. Ramezani, "Optimal perimeter control for two urban regions with macroscopic fundamental diagrams: A model predictive approach," *IEEE Transactions on Intelligent Transportation Systems*, vol. 14, no. 1, pp. 348–359, March 2013.

[21] R. Mohajerpoor, M. Saberi, H. L. Vu, T. M. Garoni, and M. Ramezani, "$\mathcal{H}^\infty$ robust perimeter flow control in urban networks with partial information feedback," *Transportation Research Part B: Methodological*, vol. 137, pp. 47–73, 2020, advances in Network Macroscopic Fundamental Diagram (NMFD) Research. [Online]. Available: https://www.sciencedirect.com/science/article/pii/S0191261518308609

[22] M. Ramezani, J. Haddad, and N. Geroliminis, "Dynamics of heterogeneity in urban networks: aggregated traffic modeling and hierarchical control," *Transportation Research Part B: Methodological*, vol. 74, pp. 1–19, 2015. [Online]. Available: https://www.sciencedirect.com/science/article/pii/S0191261515000028

[23] M. Yildirimoglu, I. I. Sirmatel, and N. Geroliminis, "Hierarchical control of heterogeneous large-scale urban road networks via path assignment and regional route guidance," *Transportation Research Part B: Methodological*, vol. 118, pp. 106–123, 2018. [Online]. Available: https://www.sciencedirect.com/science/article/pii/S0191261518301152

[24] K. Aboudolas and N. Geroliminis, "Perimeter and boundary flow control in multi-reservoir heterogeneous networks," *Transportation Research Part B: Methodological*, vol. 55, pp. 265–281, 2013. [Online]. Available: https://www.sciencedirect.com/science/article/pii/S0191261513001185

[25] K. Ampountolas, N. Zheng, and N. Geroliminis, "Macroscopic modelling and robust control of bi-modal multi-region urban road networks," *Transportation Research Part B: Methodological*, vol. 104, pp. 616–637, 2017. [Online]. Available: https://www.sciencedirect.com/science/article/pii/S0191261515300370

[26] Y. Wan, J. Cao, W. Huang, J. Guo, and Y. Wei, "Perimeter control of multiregion urban traffic networks with time-varying delays," *IEEE Transactions on Systems, Man, and Cybernetics: Systems*, vol. 50, no. 8, pp. 2795–2803, Aug 2020.

[27] T. Lei, Z. Hou, and Y. Ren, "Data-driven model free adaptive perimeter control for multi-region urban traffic networks with route choice," *IEEE Transactions on Intelligent Transportation Systems*, vol. 21, no. 7, pp. 2894–2905, July 2020.

[28] D. Li and Z. Hou, "Perimeter control of urban traffic networks based on model-free adaptive control," *IEEE Transactions on Intelligent Transportation Systems*, pp. 1–13, 2020.

[29] Z. Hou and T. Lei, "Constrained model free adaptive predictive perimeter control and route guidance for multi-region urban traffic systems," *IEEE Transactions on Intelligent Transportation Systems*, pp. 1–13, 2020.

[30] S. F. A. Batista, D. Ingole, L. Leclercq, and M. Menéndez, "The role of trip lengths calibration in model-based perimeter control strategies," *IEEE Transactions on Intelligent Transportation Systems*, pp. 1–11, 2021.

[31] I. I. Sirmatel and N. Geroliminis, "Nonlinear moving horizon estimation for large-scale urban road networks," *IEEE Transactions on Intelligent Transportation Systems*, vol. 21, no. 12, pp. 4983–4994, Dec 2020.

[32] Y. Bichiou, M. Elouni, H. M. Abdelghaffar, and H. A. Rakha, "Sliding mode network perimeter control," *IEEE Transactions on Intelligent Transportation Systems*, vol. 22, no. 5, pp. 2933–2942, May 2021.

[33] Q. Chen, C. An, J. Xia, W. Rao, and S. Li, "Feedback linearization-based perimeter controllers for oversaturated regions," *IEEE Intelligent Transportation Systems Magazine*, pp. 0–0, 2020.

[34] J. Godfrey, "The mechanism of a road network," *Traffic Engineering and Control*, vol. 11, no. 7, pp. 323–327, Nov 1969.

[35] N. Geroliminis and C. F. Daganzo, "Existence of urban-scale macroscopic fundamental diagrams: Some experimental findings," *Transportation Research Part B: Methodological*, vol. 42, no. 9, pp. 759–770, 2008. [Online]. Available: https://www.sciencedirect.com/science/article/pii/S0191261508000180

[36] N. Geroliminis, "Dynamics of peak hour and effect of parking for congested cities," *Transportation Research Board Annual Meeting 2009*, no. 09-1685, 2009. [Online]. Available: http://infoscience.epfl.ch/record/141817

[37] N. Geroliminis and J. Sun, "Properties of a well-defined macroscopic fundamental diagram for urban traffic," *Transportation Research Part B: Methodological*, vol. 45, no. 3, pp. 605–617, 2011. [Online]. Available: https://www.sciencedirect.com/science/article/pii/S0191261510001372